

1 Hydrodynamic and Biochemical Impacts on the Development of 2 Hypoxia in the Louisiana–Texas Shelf Part II: Statistical Modeling 3 and Hypoxia Prediction

4 Yanda Ou¹, Bin Li², Z. George Xue^{1,3,4}

5 ¹Department of Oceanography and Coastal Sciences, Louisiana State University, Baton Rouge, LA, 70803, USA.

6 ²Department of Experimental Statistics, Louisiana State University, Baton Rouge, LA, 70803, USA

7 ³Center for Computation and Technology, Louisiana State University, Baton Rouge, LA, 70803, USA.

8 ⁴Coastal Studies Institute, Louisiana State University, Baton Rouge, LA, 70803, USA

9 Correspondence to: Z. George Xue (zxue@lsu.edu)

10 **Abstract.** [This study presents](#) a novel ensemble regression model for hypoxic area (HA) forecast in the Louisiana–Texas
11 (LaTex) Shelf. The ensemble model combines a zero-inflated Poisson generalized linear model (GLM) and a quasi-Poisson
12 generalized additive model (GAM) and considers predictors with hydrodynamic and biochemical features. Both models were
13 trained and calibrated using the daily hindcast (2007–2020) by a three-dimensional coupled hydrodynamic–biogeochemical
14 model embedded in the Regional Ocean Modeling System (ROMS). [Compared to the ROMS hindcasts](#), the ensemble model
15 [yields a low root-mean-squared error \(RMSE\) \(3,256 km²\), a high R² \(0.7721\), and low mean absolute percentage biases for](#)
16 [overall \(29 %\) and peak HA prediction \(25 %\).](#) [When compared to the Shelf-wide cruise observations from 2012 to 2020, our](#)
17 [ensemble model provides a more accurate summer HA forecast than any existing forecast models with a high R² \(0.9200\), a](#)
18 [low RMSE \(2,005 km²\), a low scatter index \(15 %\), and low mean absolute percentage biases for overall \(18 %\), fair-weather](#)
19 [summers \(15 %\), and windy summers \(18 %\) predictions.](#) To test its robustness, the model [is](#) further applied to a global forecast
20 model and produces HA prediction from [2012](#) to 2020 with the adjusted predictors from the HYbrid Coordinate Ocean Model
21 (HYCOM). [In addition, model sensitivity tests suggest an aggressive riverine nutrient reduction strategy \(92 %\) is needed to](#)
22 [achieve the HA reduction goal of 5,000 km².](#)

23 1 Introduction

24 The Louisiana–Texas (LaTex) Shelf has become a center of hypoxia (bottom dissolved oxygen, DO < 2 mg L⁻¹) study since the
25 1980s ([e.g., Rabalais et al., 2002; Rabalais et al., 2007a; Justić and Wang, 2014](#)). Regular mid-summer [Shelf-wide](#) cruises
26 documented that the area and volume of hypoxic bottom water could reach up to 23,000 km² and 140 km³, respectively
27 (Rabalais and Turner, 2019; Rabalais and Baustian, 2020). The aquatic environments, fisheries, and coastal economies are
28 under threat of recurring hypoxia in summer (Chesney and Baltz, 2001; Craig and Bosman, 2013; [De Mutsert et al., 2016](#);
29 LaBone et al., 2020; Rabalais and Turner, 2019; Rabotyagov et al., 2014; Smith et al., 2014). [For example, habitats of some](#)
30 [fish species \(e.g., croaker and brown shrimp\) shift to offshore hypoxic edges \(Craig and Crowder, 2005; Craig, 2012\) during](#)

Deleted: In this study,

Deleted: was developed

Deleted: A promising daily HA forecast is provided by

Deleted: with

Deleted: 204

Deleted: 8005

Deleted: when compared to a precise performance in capturing hypoxic area peaks in the hindcasts

Deleted: summers

Deleted: the prevailing NOAA-supported

Deleted: was

Deleted: 2019

Deleted: The overall performance is barely acceptable. Predicted HA shows a high agreement with an R² of 0.4242, an the ROMS hindcast time series (RMSE of 5,088–4,571 km², and a SI of 38% against the Shelf-wide R²=0.8178). Our model can also predict the magnitude and onsets of summer cruise observations due to HYCOM's poor performance in water stratification HA peaks in both 2019 and 2020 with high accuracy. To the in the river-dominated shelf. A change to ROMS-derived potential energy anomaly can lead to a pronounced improvement in model predictions (R²=0.9255, RMSE=3,751 km², SI=28%). best of our knowledge, this ensemble model is by far the first one providing fast and accurate daily HA predictions for the LaTex Shelf. The model also... suggests suggests

Deleted: suggests

Deleted: harsher

Deleted: related to the

Deleted: 1980–1996 summer average

Deleted: when while considering the both hydrodynamic and biochemical effects of water stratification

Deleted: . This study demonstrates that it is feasible to perform regional ocean HA prediction using global ocean forecast

Deleted: Shelfwide

Deleted: De Mutsert et al., 2016

67 summer hypoxia events, which may impact organism energy budgets and trophic interactions (Craig and Crowder, 2005;
68 Hazen et al., 2009). The horizontal displacement of brown shrimp habitats in summer can also lead to changes in the
69 distribution of Gulf shrimp fleets (Purcell et al., 2017). Although an Action Plan has been launched by the Mississippi
70 River/Gulf of Mexico Hypoxia Task Force to control the size of the mid-summer hypoxic zone below 5,000 km² in a 5-year
71 running average since 2001 (Mississippi River/Gulf of Mexico Watershed Nutrient Task Force, 2001; 2008), hypoxic areal
72 extents experience no significant decreases in recent decades (Del Giudice et al., 2020). An accurate prediction of the hypoxic
73 area is urgently needed for coastal managers and the fishery industry.

74
75 Water column stratification and sediment oxygen consumption (SOC) are two main factors regulating the formation, evolution,
76 and destruction of bottom hypoxia from mid-May through mid-September (Bianchi et al., 2010; Conley et al., 2009; Fennel et
77 al., 2011, 2013, 2016; Feng et al., 2014; Hetland and DiMarco, 2008; Justić and Wang, 2014; Laurent et al., 2018; McCarthy
78 et al., 2013; Murrell and Lehrter, 2011; Rabalais et al., 2007b; Wang and Justić, 2009; Yu et al., 2015). The stratification
79 inhibits bottom water reoxygenation, while SOC, induced by water eutrophication associated with high anthropogenic nutrient
80 supplies by rivers, can lead to anaerobic benthic environments. Nevertheless, existing hypoxic area (HA) prediction models
81 rely most on contribution from the nutrient load rather than hydrodynamic features. Turner et al. (2006) built a multiple linear
82 regression model for summer HA prediction using the annual and May nitrogen flux (nitrate+nitrite) of the Mississippi River
83 as the predictors. The model provides a robust annual prediction when no strong wind is present but overestimates the HA in
84 windy years. Obenour et al. (2015) modeled HA using the empirical relationship between HA and bottom DO concentration
85 derived from a Bayesian biophysical model. Their model accounts for primary biophysical processes solved for steady-state
86 conditions, water transport, May total nitrogen loads by rivers, and parameterized water reaeration. Katin et al. (2022), further
87 adjusted the Bayesian model by taking into account river flows, riverine bioavailable nitrogen loadings, and wind velocity in
88 both summer (June–September) and non-summer (November–May) months. Summer riverine inputs are projected using non-
89 summer riverine variables, river basin precipitation, and river basin temperature, while summer wind velocity is resampled
90 from historical records from 1985 to 2016. Therefore, the season prediction model is known as a pseudo-forecast model since
91 predictors in future stages only include riverine inputs. This model explains 71 % and 41 %–48 % of the variability in hindcast
92 (Del Giudice et al., 2020) and geostatistically estimated HA (Matli et al., 2018), respectively. An additional Bayesian model
93 applied to summer bottom DO prediction accounts for May total nitrogen loads, distance from the Mississippi River mouth,
94 and downstream velocity (Scavia et al., 2013). The summer HA is determined by hypoxic length (HA=57.8 hypoxic length)
95 derived from summer bottom DO concentration. The model explains 69 % of the variability in observed HA by the mid-
96 summer Shelf-wide cruises. Mechanistic prediction methods have also been applied by Laurent and Fennel (2019) to develop
97 a weighted mean forecast that is calibrated using May nitrate loads and three-dimensional hindcast simulations over the period
98 1985–2018. Once calibrated, the model only requires May nitrate loads as an input to produce the seasonal forecast for a given
99 year. The model can explain up to 76 % of the year-to-year variability of the HA observation. However, the model is not
100 favorable for years with strong wind events during summer.

Deleted: can be informative for

Deleted: deconstruction

Deleted: which is

Deleted: However

Deleted: prevailing

Deleted: for the hypoxic area (HA)

Deleted: -induced

Deleted: mechanisms

Deleted: However, prevailing prediction models for the hypoxic area (HA) rely most on nutrient-induced mechanisms rather than the hydrodynamic features. Turner et al. (2006) built a multiple linear regression model for summer HA prediction models for the hypoxic area (HA) rely most on nutrient-induced mechanisms rather than the hydrodynamic features. Turner et al. (2006) built a multiple linear regression model for summer HA using the annual and May nitrogen flux (nitrate+nitrite) of the Mississippi River as the predictors. The model provides a robust annual prediction using the annual and May nitrogen flux (nitrate+nitrite) of the Mississippi River as the predictors. The model provides a robust annual prediction when no strong wind was present but underestimates the HA in windy years.

Deleted: by

Deleted: accounted

Deleted: ,

Deleted: Katin et al. (2021)

Deleted: , however,

Deleted: The pseudo-forecast

Deleted: Another

Deleted: was proposed for

Deleted: concentration

Deleted: taking account of

Deleted: Shelfwide cruises. Different from linear regression and Bayesian analysis,

Deleted: developed

Deleted: method

Deleted: on the

Deleted: (

Deleted:).

Deleted: the

Deleted: for the forecast year as the only

Deleted: .

141 These above-mentioned models share some similar **drawbacks**. (1) The effects of water column stratification are considered
 142 **only implicitly by the associated wind speeds, water transport, and riverine nutrient loads (usually correlated to river**
 143 **discharges), although** stratification is documented as a crucial factor in regulating HA variability. (2) **Forecast of the predictors**
 144 **is usually limited, which restricts some of these seasonal models to pseudo ones.** (3) Most models **are only capable of capturing**
 145 **interannual** HA variability and **are not reliable in summers when winds are strong**. According to the hindcast results by our
 146 three-dimensional coupled hydrodynamic–biogeochemical model described in the accompanying paper (Part I), **strong wind**
 147 **events bring considerable uncertainties to** monthly and daily variabilities of HA. **In this study, we aim to provide a novel HA**
 148 **prediction method that considers** both stratification and biochemical effects. **Our new model aims to produce daily HA**
 149 **forecasts based on selected predictors' forecasts with a minimum computational cost.** The rest of the paper is organized as
 150 follows. **Detailed descriptions** of methods and data **are given in section 2. The employments** of generalized linear models
 151 (GLMs), **generalized additive models (GAMs), and an independent model application using a global forecast product (HYbrid**
 152 **Coordinate Ocean Model, HYCOM; Bleck and Boudra, 1981; Bleck, 2002), are given in section 3. Comparisons against**
 153 **existing forecast models, recommendations on nutrient reduction strategy, and model improvement outlook are given in section**
 154 **4.**

155 2 Methods

156 2.1 Data preparation

157 We adapted a three-dimensional coupled hydrodynamic–biogeochemical model embedded in the framework of the Regional
 158 Ocean Modeling System (ROMS) on the platform of Coupled Ocean–Atmosphere–Wave–Sediment Transport **Modelling**,
 159 system (COAWST, Warner et al., 2010) to the GoM (Gulf–COAWST, for detailed descriptions, validations, and results of the
 160 numerical model see Part I). Numerical hindcasts (hereafter denoted as ROMS hindcasts or ROMS simulations) are output
 161 daily from 1 January 2007 to 26 August 2020 and spatially averaged over the LaTex Shelf **extending from the west of**
 162 **Mississippi River mouth to 95°W with water depths ranging from 6 to 50 m (color shaded region in Figure A1b).**

163 2.1.1 Hydrodynamic-related predictors

164 Both water stratification and bottom biochemical processes modulate the variability of bottom DO concentration in the LaTex
 165 Shelf. Potential energy anomaly (PEA, in J m^{-3}) is introduced as an estimate of water column stratification according to:

$$167 \text{PEA} = \frac{1}{H} \int_{-h}^{\eta} (\rho - \rho) g z dz, \quad (1)$$

168
 169 where ρ is water density profile (estimated by water temperature and salinity profiles) over water column of depth $H = h + \eta$,
 170 h is the location of the bed, η is water surface elevation, g is the gravitational acceleration (9.8 m s^{-2}), z is the vertical axis, ρ

- Deleted:** ¶
- Deleted:** shortages:...(1) The effects of water column stratification are not included or only partially ...onsidered only implicitly by the associated wind speeds, water transport, and riverine nutrient loads (usually correlated to river discharges), although even though ... [1]
- Deleted:** ...2) Information onThe information of future conditions of ... [2]
- Deleted:** is limited a although some models are built upon multiple predictors, thus these forecast models
- Deleted:** are indeed "pseudo-forecast" ones.
- Deleted:**
- Deleted:** capture
- Deleted:** year-to-year...HA variability and fail whenever w... [3]
- Deleted:** favorable for
- Deleted:** reliable
- Deleted:** strong summer
- Deleted:** in summerin summers
- Deleted:** cannot be neglected before and after strong wind events... Here ... [4]
- Deleted:** In this study,...we aimed ... [5]
- Deleted:** new ...ovel HA prediction technique ...ethod in HA prediction that ... [6]
- Deleted:** considering
- Deleted:** , and... Our new model aims to produce accurately producesexecuting ...aily HA forecasts of HA ... [7]
- Deleted:** the forecasts of ...elected predictors' forecasts with a minimum computational...omputational cost.predictors. ... [8]
- Deleted:** An important assumption is that the future conditions of predictors are accessible. Indeed, it can be fulfilled by using global forecast products such as the HYbrid Coordinate Ocean Model (HYCOM)), which provides operational hydrodynamics forecasts for up to one week (eight days), or using regional models (lik... [9]
- Deleted:** : a detailed description ...of methods and data ... [10]
- Deleted:** and the ensemble model) ...nd an independent n... [11]
- Deleted:** (...leek and Boudra, 1981;)...Ci...ADDIN ... [12]
- Deleted:** products
- Deleted:** is given in section 3. The ensemble HA predictio... [13]
- Deleted:** prevailing
- Deleted:**
- Deleted:** will beis discussed afterwardin section 4.
- Deleted:** descriptions
- Deleted:** modeling
- Deleted:** a range of depth
- Deleted:** .
- Deleted:** In this study, we aimed to produce a fast and acc... [14]

375 is the depth-integrated water density given by $\rho = \frac{1}{H} \int_{-h}^{\eta} \rho dz$ (Simpson and Hunter, 1974; Simpson et al., 1978; Simpson,
 376 1981; Simpson and Bowers, 1981). The PEA represents the amount of energy per volume **required** to homogenize the entire
 377 water column (Simpson and Hunter, 1974). Thus, a greater PEA value represents a more stratified water column. As a river-
 378 dominated area, water stratification in the LaTex Shelf is highly affected by freshwater-induced buoyancy from the Mississippi
 379 and Atchafalaya Rivers. Sea surface salinity (SSS) is a good proxy **for** representing the distribution and variability of river
 380 freshwater across the shelf. Indeed, the correlation of regionally averaged PEA and SSS is significantly high **as** -0.87 ($p < 0.001$;
 381 Figure 1a) which emphasizes the importance of freshwater-induced stratification. Therefore, we considered SSS as another
 382 candidate predictor besides PEA.

384 **Surface heating and wind mixing are two other factors that influence water stratification (Simpson, 1981). The tidal effects**
 385 **considered in Simpson (1981) are neglected here due to the relatively weaker contribution in stratification in the shelf when**
 386 **compared to the effects of rivers and winds. The two mixing terms are quantified as follows:**

$$388 \frac{d(PEA)}{dt} = \frac{\alpha g}{2c} Q - \delta k_a \rho_a W^3, \quad (2)$$

389 where Q is the rate of surface heat input, α is the volume expansion coefficient, c is water specific heat capacity, δ is a
 390 coefficient of wind mixing, k_a is drag coefficient, ρ_a is humid air density near the sea surface, and W is the wind speed near
 391 the sea surface. The first term on the right-hand side of Eq. (2) represents the rate of change of water stratification due to
 392 surface heating, while the second term is the rate of working by wind stress contributing negatively to water stratification.
 393 Therefore, the heat-induced change of PEA is proportional to **surface** heat input, which is,

$$396 d(PEA)_{heat} \propto Q, \quad (3)$$

398 The total net heat flux, a sum of net shortwave and net longwave radiation flux, is derived from the National Centers for
 399 Environmental Prediction Climate Forecast System (NCEP) Reanalysis (CFSR) 6-hourly products (Saha et al., 2010; 2011) in
 400 this study. The term Q is added to the candidate list of predictors and is denoted as PEA_{heat} (heat-induced PEA changes) for
 401 simplification (Figure 1a).

403 Daily variability of term $(\delta k_a \rho_a W^3)$ is dominated by that of W^3 , since the ρ_a fluctuates much less than the W^3 **on** a daily
 404 scale (Figure A2). We obtained the ρ_a according to (Picard et al., 2008) :

$$406 \rho_a = \frac{p M_a}{z R T} \left[1 - x_v \left(1 - \frac{M_v}{M_a} \right) \right], \quad (4)$$

407

Deleted: Simpson and Hunter, 1974;

Deleted: Simpson et al., 1978

Deleted: Simpson and Hunter, 1974

Deleted: in

Deleted: up to

Deleted: 88

Deleted: In the meantime, s

Deleted: can be

Deleted: In the meantime, surface heating and wind mixing are other two factors influencing water stratification (Simpson and Hunter, 1974; Simpson et al., 1978) and can be quantified as follows:...

Deleted: $\frac{\alpha g h}{2c}$

Deleted: the product of

Deleted: and water depth

Deleted: $Qh, \rightarrow \rightarrow \rightarrow \rightarrow \rightarrow \rightarrow \rightarrow \rightarrow \rightarrow$

Deleted: (Qh)

Deleted: .

Deleted: in

Deleted: A1

428 where p represents the absolute air pressure, M_d ($=28.96546 \text{ g mol}^{-1}$) is the molar mass of dry air, M_v ($=18.01528 \text{ g mol}^{-1}$) is
 429 the molar mass of water vapor, Z indicates compressibility, R ($=8.314472 \text{ J mol}^{-1} \text{ K}^{-1}$) is the molar gas constant, T is
 430 thermodynamic temperature, x_v is the mole fraction of water vapor. We assumed that air parcels at the sea surface are ideal
 431 gases ($Z = 1$) and are always saturated with water vapor. Thus, x_v is a function of absolute air pressure (p) and saturation
 432 vapor pressure of water (p_{sat}) and can be calculated as follows:

$$434 \quad x_v = \frac{p_{sat}}{p}, \quad (5)$$

436 According to the adjusted Tetens equation (Murray, 1967; Monteith and Unsworth, 2014), p_{sat} (in Pa) can be estimated by:

$$438 \quad p_{sat} = 611 e^{\frac{17.27(T-237.3)}{T-T'}}, \quad (6)$$

440 where $T' = 36 \text{ K}$. Substitute Eqs. (5)–(6) to Eq. (4) with the assumption of $Z = 1$, we obtained air density as a function of both
 441 air pressure and air temperature in the following:

$$443 \quad \rho_a = \rho_a(T, p) = \frac{pM_d}{RT} \left[1 - \frac{611}{p} \left(1 - \frac{M_v}{M_d} \right) e^{\frac{17.27(T-237.3)}{T-T'}} \right], \quad (7)$$

445 The ρ_a is then estimated using sea surface air pressure and air temperature 2 meters above the sea surface provided by NCEP
 446 CFSR 6-hourly products. The correlation of daily $\rho_a W^3$ and W^3 (provided by NCEP CFSR 6-hourly products) is significantly
 447 high as 0.9988 ($p < 0.001$, Figure A2) emphasizing the importance of term W^3 in controlling the daily variability of wind-
 448 induced PEA changes over the shelf. We, thus, approximated the relationship as:

$$450 \quad d(PEA)_{wind} \propto W^3, \quad (8)$$

452 The term W^3 is introduced as another candidate predictor and is denoted as PEA_{wind} (wind-induced PEA changes) for
 453 simplification (Figure 1a).

454 2.1.2 Biochemical-related predictors

455 Sedimentary biochemical processes directly influence the bottom DO consumption rate. However, global forecast models such
 456 as HYCOM do not cover biochemical parameters. Therefore, the biochemical-related term SOC needs to be replaced by an
 457 alternative term (denoted as SOCalt). According to the SOC scheme (Eq. 9) stated in Part I, the biochemical features are
 458 attributed to the sedimentary particulate organic nitrogen concentration (PONsed, derived from ROMS hindcasts). The total

Deleted: According to the Tetens equation (Monteith and Unsworth, 2014), p_{sat} (in Pa) can be estimated for the following:

Deleted: $610.78 e^{\frac{17.27(T-237.3)}{T}}$, $\rightarrow \rightarrow \rightarrow \rightarrow \rightarrow \rightarrow \rightarrow \rightarrow$

Deleted: $\frac{pM_d}{ZRT} \left[1 - \frac{1}{p} \left(1 - \frac{M_v}{M_d} \right) e^{\frac{17.27(T-237.3)}{T}} \right]$, $\rightarrow \rightarrow \rightarrow \rightarrow \rightarrow \rightarrow \rightarrow$

Deleted: Correlation

Deleted: 9989

Deleted: A1

Deleted: .

Deleted: by far,

Deleted: model systems like

Deleted: does

Deleted: simulateinclude

Deleted: fields

Deleted:) that does not rely on biochemical simulations.

Deleted: stated in

Deleted: (8) and Eq. (10)

Deleted: concentration

476 nitrate+nitrite loads by the Mississippi River are used to represent the PONsed variability due to the long-term data supports.
 477 The daily Mississippi River discharges at site 07374000 are updated daily by the U.S. Geological Survey (USGS) National
 478 Water Information System (NWIS) since March 2004. The total nitrogen concentration at site 07374000 is provided and
 479 updated daily by USGS since November 2011. Prior to 2011, nitrogen loads (at site 07374000) are provided monthly by USGS
 480 and, in this study, are interpolated to daily intervals according to the corresponding monthly loads. Although phosphate and
 481 silicate are another two limitation nutrients in the shelf, daily measurement are still not available for the Mississippi River.
 482 Monthly total nitrate+nitrite loads, phosphate loads, and silicate loads by both the Mississippi River and the Atchafalaya River
 483 are significantly correlated (Table A1). Therefore, the total nitrate+nitrite loads applied here can be interpreted as total nutrient
 484 loads by both river systems. Due to lateral transports and vertical settling of particulate organic matter, a leading period should
 485 be introduced to the time series of riverine nutrient loads. The optimal length of leading days is obtained by examining the
 486 highest linear correlation of regionally averaged ROMS-hindcast SOC and SOCalt (Eq. (10)) and is calculated as 44 days
 487 ($R=0.7427, p<0.001$, Figure A3a). The exponential term in Eqs. (9)–(10) estimates the temperature-dependent decomposition
 488 rate of organic matter.

$$489 \text{SOC} = \text{PON}_{\text{sed}} \cdot \text{VP}2N_0 \cdot e^{K_{P2N} \cdot T_b} \quad (9)$$

$$490 \text{SOCalt} = \text{Mississippi River inorganic nitrogen loads (led by 44 days)} \cdot e^{0.0693T_b} \quad (10)$$

492 $\text{VP}2N_0$ is a constant representing the decomposition rates of sedimentary particulate organic nitrogen, PON_{sed} , at 0 °C. K_{P2N}
 493 is a constant (0.0693 °C⁻¹) indicating temperature coefficients for decomposition of PON_{sed} . T_b is bottom water temperature
 494 (in °C). The Q10 (= 2 given the above chosen coefficients; van't Hoff and Leffeldt, 1899; Reyes et al., 2008) assumption is
 495 applied to mimic the aerobic decomposition rate of PON_{sed} . Along with SOCalt, the temperature-dependent decomposition
 496 rate $e^{0.0693T_b}$ is also considered as a candidate predictor in statistical models and is denoted as DCP_{Temp} for simplification.

497 2.1.3 HA estimation

498 As listed in Table 1, six candidate predictors are considered in the statistical models including four stratification-related
 499 variables (PEA, SSS, PEA_{heat} , and PEA_{wind}) and two bottom biochemical variables (SOCalt and DCP_{Temp}). The correlation
 500 coefficient matrix (Figure 1a) indicates that multicollinearity may become a problem in regression models since linear
 501 correlations among some predictors are significantly high, e.g., 0.74 ($p<0.001$) between PEA and SOCalt, and -0.87 ($p<0.001$)
 502 between PEA and SSS. The multicollinearity can harm the assumption that predictors are independent. It can lead to difficulties
 503 in individual coefficients test and numerical instability (Siegel and Wagner, 2022). The frequency distribution of HA (Figure
 504 1b) illustrates that the response variable is highly right-skewed with ~42% of samples (2,081 out of 4,943) being exactly zero.
 505 The HA is estimated by the number of hypoxia cells (ROMS computational cells reaching hypoxic conditions) times a nearly
 506 constant value (area of the computational cell), which is $25.56 \pm 0.17 \text{ km}^2$ (mean \pm 1SD). Thus, the HA can be estimated by
 507 the number of grid cells when the Poisson and negative binomial regression models are applied. However, the great portion of
 508 zero samples leads to overdispersion (magnitude of variance \gg magnitude of mean, i.e., 45,730,441 \gg 4,507) and zero-

Deleted: and

Deleted: also ...rovided and updated daily by the ...SGS since November 2011. Prior to 2011, nitrogen loads (at site 07374000) are provided monthly by USGS and, in this study, are extended (... [15])

Deleted: interpolated

Deleted: series by assigning the monthly loads to days within the corresponding months

Deleted: s...ing water discharge (... [16])

Deleted: Daily nitrate+nitrite loads can be estimated by the product of the daily Mississippi River discharges and daily nitrate+nitrite concentration.

Deleted: load by the Mississippi River are used to represent the PONsed variability

Deleted: other...nother two limitation nutrients in the shelf, daily updates of data are...easurement are still ...ot available for the Mississippi River. On the other hand, m (... [17])

Deleted: , ...because inorganic nitrogen is the primary nutrient resource for plankton bloom. Daily updates of measured riverine nitrate+nitrite loads are accessible from U.S. Geological Survey (USGS) National Water Information System (NWIS). ...ue to lateral transports and vertical settling of particulate organic matter, a leading period should be introduced to the time series of riverine nutrient loads. The optimal length of leading days is obtained by examining the highest linear correlation of regionally averaged ROMS-hindcast SOC and SOCalt (following ...q, (109...)) and is calculated as 4419...days ($R=0.7427, p<0.001$, Figure A2a...3a). The exponential term in EqsEq... (9)–(10) estimates the temperature-dependent decomposition rate of organic matter. A significant correlation coefficient between daily SOCalt and ROMS-hindcast SOC is found as 0.8157 ($p<0.001$, Figure A2). (... [18])

Deleted: †

Deleted: (led by 19 days) $\cdot e^{0.0693T_b}$ $\rightarrow \rightarrow \rightarrow$ (...09 (... [19])

Deleted: where indicates ...ottom water temperature (in °C). The Q10 (= 2 given the above chosen coefficients; van't Hoff and Leffeldt, 1899; (...eyes et al., 2008) (... [20])

Deleted: there are

Deleted: As listed in Table 1, there are six candidate predictors considered in the statistical models including four stratification-related variables (PEA, SSS, (Qh), and W^3) and two bottom biochemical variables (SOCalt and $e^{0.0693T_b}$). For simplification, we denoted this variable as (Qh), W^3 , and $e^{0.0693T_b}$ as PEA_{heat} , PEA_{wind} , and DCP_{Temp}

Deleted: , respectively. Correlation...coefficients...matrix (Figure 1a) indicates that multicollinearity may become a problem in regression models since linear correlations among some predictors are significantly high, e.g., 0.7476... ($p<0.001$) between PEA and SOCalt, and -0.8788... ($p<0.001$) between PEA and SSS. The multicollinearity can harm the assumption that predictors are independent. It can lead to difficulties in individual coeffi (... [21])

Deleted:)...Thus, the HA can be estimated by the number of grid cells when the Poisson and negative binomial regression mo (... [22])

Deleted: m...magnitude of mean, i.e., 45,730,44152,161,... [23])

Deleted: 378

634 inflated problems (Lambert, 1992). The overdispersion issue violates the mean-variance equality assumption employed in
 635 regular Poisson regression models, while zero-inflated problems can weaken the model performances.

636 **Table 1. Description of daily response variable and candidate predictors. The data cover a time range from 1 January**
 637 **2007 to 26 August 2020. Prescribed min and max are used for min-max normalization.**

Variables [units]	Description	Min	Median	Mean	Max	Prescribed (Min:Max)	
HA [km ²]	<u>Hypoxic area (when bottom dissolved oxygen ≤ 2 mg L⁻¹)</u>	0	<u>1.137</u>	<u>4.507</u>	<u>34.097</u>	Non-normalized	Deleted: 0 Deleted: 378 Deleted: 40,561 Deleted: Area of extremely low concentration (< 1)
PEA [J m ⁻³]	Potential energy anomaly measuring the water stratification	<u>3.3</u>	<u>35.6</u>	<u>47.2</u>	<u>187.9</u>	(0:200)	Deleted: 36.9 Deleted: 49 Deleted: 190.4
SSS [non-dim]	Sea surface salinity	<u>20.0</u>	<u>30.8</u>	<u>30.4</u>	<u>33.9</u>	(0:40)	Deleted: 7
PEA _{heat} [W m ⁻³]	= Q_s , an approximation of surface heat-induced water stratification	<u>-54.4</u>	<u>151.9</u>	<u>142.7</u>	<u>261.3</u>	(-60:300)	Deleted: 31 Deleted: 31 Deleted: 34.4 Deleted: Q_h
PEA _{wind} [m ³ s ⁻³]	= W^3 , an approximation of water stratification changes due to wind mixing	<u>0.5</u>	<u>164.7</u>	<u>296.1</u>	<u>7013.2</u>	(0:7,100)	Deleted: 1,472.9 Deleted: 3,986.3 Deleted: 3,717.2 Deleted: 6,829.7 Deleted: 2,000:7,000
SOC _{alt} [mmol s ⁻¹]	An alternative term for sediment oxygen consumption.	<u>789.31</u>	<u>10,423.3</u>	<u>13,377.2</u>	<u>41,984.0</u>	(<u>770,000:43,000</u>)	Deleted: 8 Deleted: 175.1 Deleted: 305.4 Deleted: 6,415.8 Deleted: 6,500
DCP _{Temp} [non-dim]	= $e^{0.0693 \cdot T_b}$, temperature-dependent decomposition rate of organic matter	2.6	5.1	5.2	8.0	(0:10)	Deleted: m ³ Deleted: 800 Deleted: 42 Deleted: 874,870 Deleted: 103,864 Deleted: 12,604,970 Deleted: 530,153

638

671 **2.2 Data pre-processes**

672 We first spatially averaged ROMS-derived predictors (daily) over the LaTex Shelf (color-shaded area in Figure A1b), then
 673 applied the min-max normalization (Eq. (11)) to the one-dimensional time series. Predictive models can be beneficial from the
 674 min-max normalization when applying to a new dataset since the method guarantees that the normalized predictors from
 675 different datasets range from 0 to 1 as the minimum and maximum values are prescribed. Note that the response is not
 676 normalized.

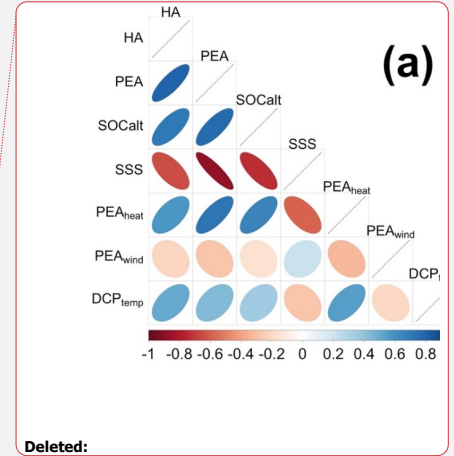
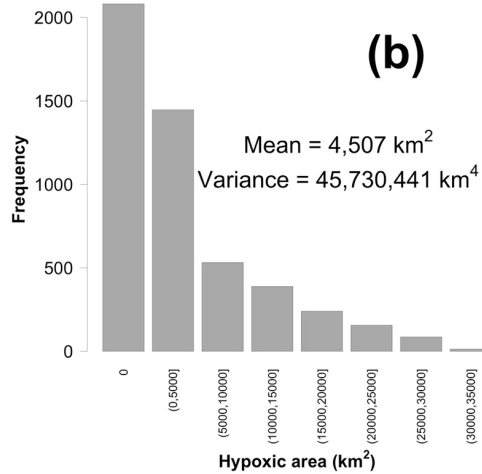
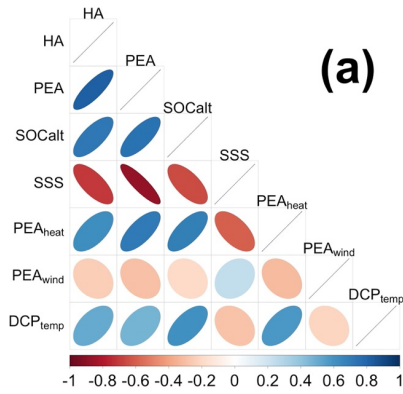
677
 678
$$X_{nor} = \frac{X_{org} - Min_{prescribed}}{(Max_{prescribed} - Min_{prescribed})}, \quad (11)$$

 679

680 where X_{nor} , X_{org} , $Min_{prescribed}$, and $Max_{prescribed}$ represent normalized value, original value, prescribed minimum, and
 681 prescribed maximum, respectively. The daily samples are then split into a training set (for model construction) accounting for
 682 80 % of the total samples and a test set (for assessment of model performances) accounting for the remaining 20 %. To maintain
 683 the HA distribution in both sets, a random resampling method is applied in different HA intervals individually. For example,
 684 80 % of samples with HA=0 are chosen randomly for the training set out of all daily samples with HA=0, while the rest of the
 685 samples with HA=0 are grouped into the test set. The HA=0 is the first interval to which the resampling process is applied,
 686 while the remaining samples are split at intervals of 5,000 km². However, the distribution of HA from each year is similar with
 687 a right-skewed structure and numerous zero values. Thus, even through random processes, both the training and test sets
 688 contain samples from each year including samples with non-peak and peak HA. This splitting method increases the model
 689 applicability and provides a comprehensive assessment of prediction performances on both non-peak and peak HA.

- Deleted: applied
- Deleted: to daily
- Deleted: the spatially averaged daily ROMS-derived predictors over the LaTex Shelf,
- Deleted: -
- Deleted: 10
- Deleted: -
- Deleted: 10

- Deleted: rest
- Deleted: is
- Deleted: is
- Deleted: rest of
- Deleted: every
- Deleted: though
- Deleted: Samples shown in Figure 4 are listed sequentially in the time dimension from 2007 to 2020 but are not equally distributed along time, which means that the listed samples should not be regarded as time series.



Deleted:

Deleted: C

709
710 **Figure 1. (a) A correlation coefficient matrix of the response variable and candidate predictors, and (b) the frequency distribution**
711 **of HA. Data are provided daily from 1 January 2007 to 26 August 2020.**

712 **2.3 Model skill assessment**

713 The R^2 , root-mean-square error (RMSE), mean absolute percentage bias (MAPB), and scatter index (SI; Zambresky, 1989)
714 are used to assess the model performances in HA predictions. The SI is a normalized measure of error or a relative percentage
715 of expected error with respect to the mean observation. The calculations of the statistics are given in Eqs. (12) – (15).

716
$$R^2 = 1 - \frac{\sum_{i=1}^N (P_i - O_i)^2}{\sum_{i=1}^N (P_i - \bar{O})^2} \quad (12)$$

717
718
$$RMSE = \sqrt{\frac{\sum_{i=1}^N (P_i - O_i)^2}{N}} \quad (13)$$

719
720
$$MAPB = \frac{1}{N} \sum_{i=1}^N \left| \frac{P_i - O_i}{O_i} \right| \times 100\% \quad (14)$$

721
722
$$SI = \frac{RMSE}{\bar{O}} \times 100\% \quad (15)$$

723 where P_i and O_i represent the i th record of prediction and observation (or hindcast), while \bar{O} represents the average of all
724 observed (or hindcast) records.

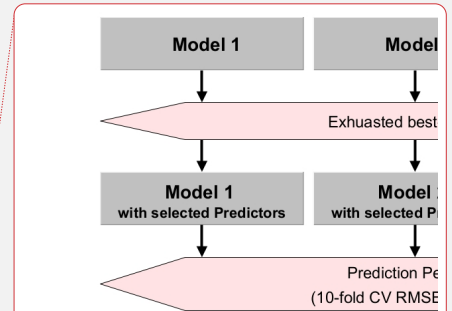
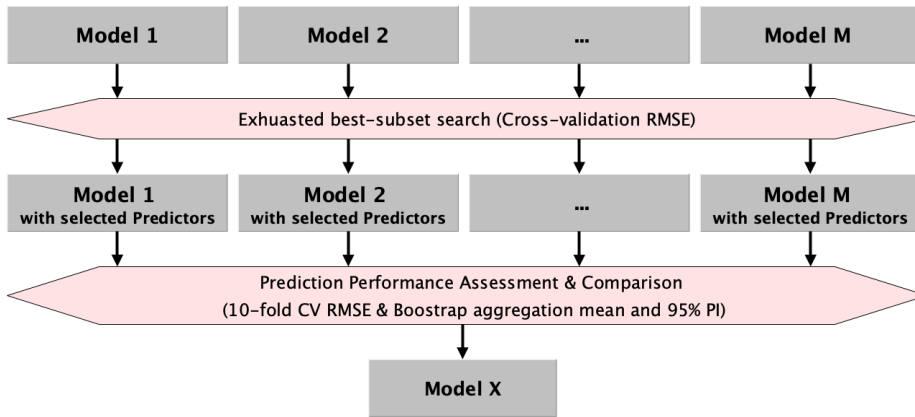
727 **3 Model construction and results**

728 **3.1 Model built-up process**

729 Several regression models are explored using the statistical programming language R. To find the “best” model balancing both
 730 model interpretability and prediction performance, a procedure is conducted for model selection (Figure 2) and is summarized
 731 below. (1) Choose a regression model. (2) Apply an exhaustive best-subset searching approach to the chosen model. Models
 732 with possible combinations of candidate predictors from the ROMS training set are built. A 10-fold cross-validation (CV)
 733 method is applied to each model yielding 10 RMSEs and 1 corresponding mean. The candidate predictors of PEA and SOCal
 734 are forced into each subset. Thus, the number of fitted models with a subset size of k is $C(6 - 2, k - 2) = \frac{4!}{(6 - k)!(k - 2)!}$, $2 \leq$
 735 $k \leq 6$ (the total number of candidate predictors is 6). The optimal subset of this size is found as the one with the lowest mean
 736 CV RMSE among these models. The best subset is then obtained by comparing mean CV RMSEs of the optimal subsets of
 737 different sizes. (3) Steps (1)–(2) are repeated for the selected M candidate regression models. (4) Prediction performances of
 738 different models with the corresponding best subsets are assessed by the 10-fold CV RMSEs and Bootstrap (1,000 iterations)
 739 aggregating (i.e., Bagging) ensemble algorithms. The Bagging method builds the given model N ($=1,000$) times during each
 740 of which the given model is trained using different samples chosen randomly and repeatedly from the ROMS training set and
 741 is executed for HA prediction using samples in the ROMS test set. The ensemble means and ensemble 95 % prediction intervals
 742 (PIs) of forecast HA are given according to the prediction results in the 1,000 iterations. The best model (Model X in Figure
 743 2) is chosen according to the comparisons of the 10-fold CV RMSEs and the Bagging results.

Deleted: root-mean-square errors (
 Deleted:)

Deleted: i



Deleted:

745
 746

Figure 2. A flow chart of building up regression models.

3.2 Generalized linear models (GLMs)

Deleted: ¶

3.2.1 Regular GLMs and zero-inflated GLMs

The response variable can be treated as count data. Regular Poisson (function `glm` in R package “stats” version 3.6.2), quasi-Poisson (function `glm` in R package “stats” version 3.6.2), and negative binomial (function `glm.nb` in R package “MASS” version 7.3-54; Venables and Ripley, 2002) GLMs are explored in this section. The latter two GLMs are known for solving overdispersion problems by relaxing the mean-variance equality assumption. These GLMs make use of a natural log link function. Thus, a natural logarithm of the area of a single ROMS cell (~ 25.56 km²) is added to the models as an offset term (an additional intercept term).

In addition, the overdispersion issue can result from the great percentage (~42%) of zero values in the response variable (Figure 1b). Zero-inflated GLMs (using function `zeroinfl` in R package “pscl” version 1.5.5; Jackman, 2020; Zeileis et al., 2008) are developed for dealing with response variables of this kind. Rather than resetting dispersion parameters, a zero-inflated count model is a two-component mixture model blending a count model and a zero-excess model. The count model is usually a Poisson or negative binomial GLM (with log link), while the zero-excess model is a binomial GLM (with logit link in this study) estimating the probability of zero inflation. An offset term of $\log(25.56)$ is also introduced into the count model. Instead of applying the best-subset searching to the count and zero-excess models simultaneously, in this study, the searching is conducted respectively for these two models to reduce the demands of computational resources. The best subset of the zero-excess model (binomial GLM) is given first. The best subset of the count model (Poisson or negative binomial GLMs) is then provided blending the zero-excess model with the corresponding selected best subset fixed.

Deleted: 51

However, it is hard to determine whether a given zero value of HA is excessive, instead, it is relatively easy to model hypoxia occurrence assuming that all the zero values are excessive. A new binary response, hypoxia, stated in Eq. (16) is introduced for modeling hypoxia occurrence using regular binomial GLMs (function `glm` in R package “stats” version 3.6.2). The hypoxia is equal to 0 when HA is 0 (no hypoxia), otherwise, is equal to 1. The optimal model selected three predictors: PEA, SOCalt, and DCP_{Temp} (Figure 3b).

Deleted: 11

Deleted: model

Deleted: odelling

Deleted: ed

$$\text{hypoxia} = \begin{cases} 0, & \text{no hypoxia} \\ 1, & \text{hypoxia occurs} \end{cases}$$

(16)

Deleted: 11

3.2.2 Performance of GLMs

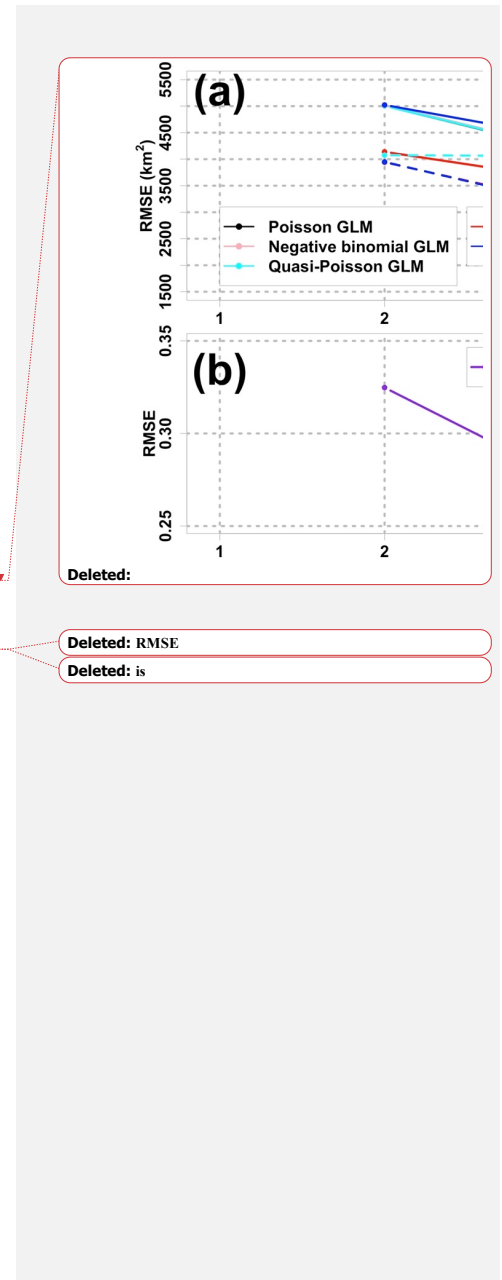
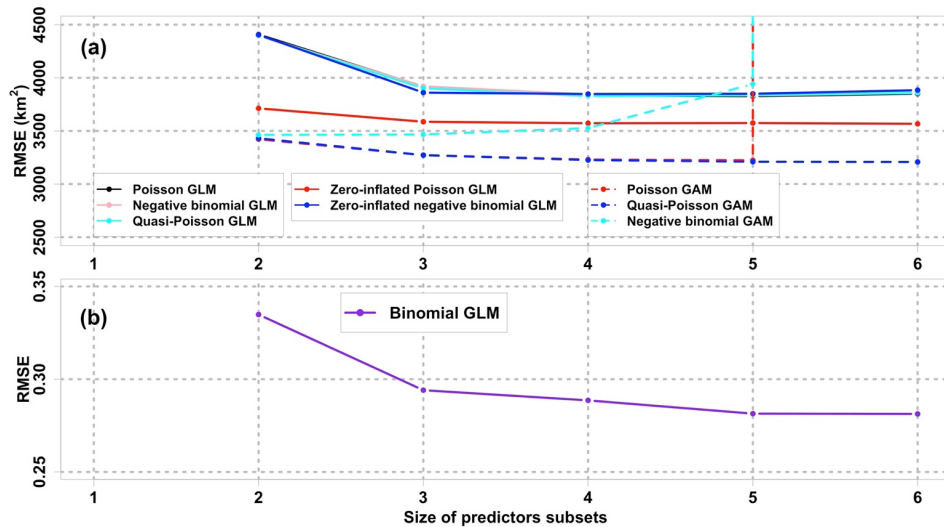
The zero-inflated Poisson GLM serves as the best GLM in terms of prediction performances since it has the lowest mean CV RMSE (Figure 3a) among the five candidates GLMs. The relaxation of the mean-variance equality assumption by the negative

Deleted: candidate

790 binomial GLM and the quasi-Poisson GLM does not guarantee salient improvement of performances when comparing their
 791 CV RMSEs to those of regular Poisson GLM. The zero-inflated negative binomial GLM yields **similar performances to the**
 792 **three regular GLMs**. The mean CV RMSEs of zero-inflated Poisson GLM hit the trough (3,573 km²) at the size of **four**.
 793 However, the greatest drop of RMSEs (3,586 km²) occurs at the size of three beyond which the RMSEs remain stable. It is
 794 worth considering a model with fewer predictors satisfying model interpretability. Thus, the best zero-inflated Poisson GLM
 795 accounts for three predictors (PEA, SOCal, and DCP_{Temp}) in the count model and three predictors (PEA, SOCal, and DCP_{Temp})
 796 in the zero-excess model. As indicated in the correlation matrix (Figure 1a), the robustness of a model can be **impaired** by
 797 multicollinearity which can be estimated by variance inflation factors (VIFs). VIFs among the selected predictors are 2.15,
 798 2.70, and 1.59 for PEA, SOCal, and DCP_{Temp}, respectively. The VIFs are all less than 5 suggesting that **both the count and the**
 799 **zero-excess models with these predictors involved are** merely violated by multicollinearity. For simplicity, the best zero-
 800 inflated Poisson GLM is symbolized as GLMzip3.

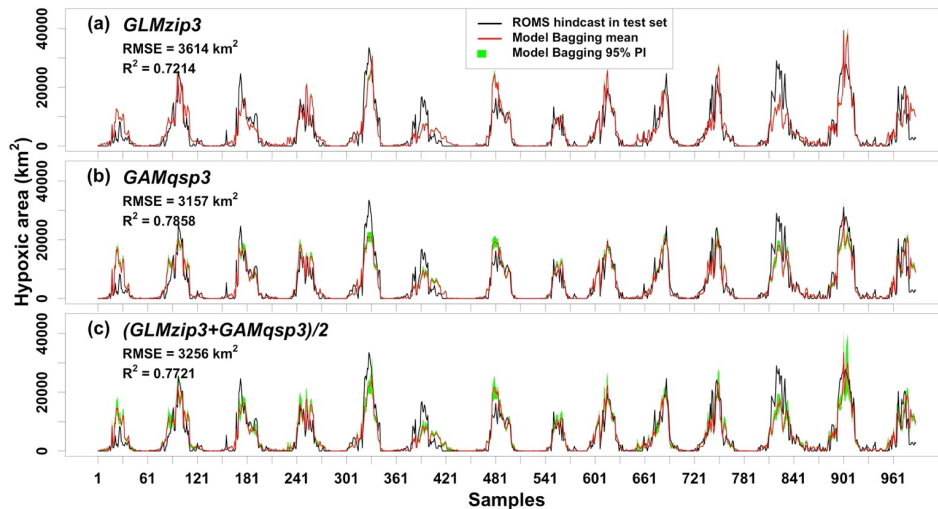
801
 802 The Bagging ensemble method is implemented to estimate the prediction performance of GLMzip3 (Figure 4a). **It is noted**
 803 **that the training set and test set are resampled according to different HA intervals. Since the distributions of HA in each year**
 804 **are similar (see Section 2.2), HA in both training and test set contains observations of peak and non-peak values in each year.**
 805 **Therefore, samples shown in Figure 4 are listed sequentially in the time dimension from 2007 to 2020 but are not necessarily**
 806 **evenly distributed. The listed samples should not be regarded as time series.** The Bagging means of predicted HA provides an
 807 RMSE of 3,614 km² and an R² of 0.7214 against the ROMS hindcasts. The Bagging 95 % PIs are restricted within a narrow
 808 range with a slight increase at the predicted peaks. **Within different ranges of hindcast HA, the MAPB between predicted and**
 809 **hindcast HA ranges from 29 % to 38 % with an average of 33 % (Table 2). Particularly, the GLMzip3 produces the lowest**
 810 **bias (29 %) for the hindcast HA ≥ 30,000 km².** The results suggest that GLMzip3 is capable of providing not only accurate
 811 but also stable HA forecasts. Nevertheless, we noted salient overestimations (e.g., **peaks around samples 30, 481, and 901**) and
 812 underestimations (e.g., **peaks around samples 181, 390, and 826**) at some peaks. Instead of the prediction performance at non-
 813 peak HA, here we **focused more on the** forecasts at HA peaks which impose more **threats** to the shelf ecosystem. In section
 814 3.3, GAMs are investigated with an expectation of further improvements in peak predictions by considering non-parametric
 815 or non-linear effects of the predictors.

- Deleted:** poorest performance with
- Deleted:** largest mean CV RMSE.
- Deleted:** 621
- Deleted:** five
- Deleted:** 671
- Deleted:** impaired
- Deleted:** 60
- Deleted:** 43
- Deleted:** 23
- Deleted:** predictors subsets involved in both the count and the zero-excess models are
- Deleted:** the
- Deleted:** set
- Deleted:** equally
- Deleted:** along time
- Deleted:** 610
- Deleted:** 7511
- Deleted:** i
- Deleted:** of the predicted values
- Deleted:** We want to address that the comparisons are not
- Deleted:** the time series. The training set and test set are resampled according to different HA intervals, while the distributions of HA in each year are similar. Thus, HA in both the training set and test set contains observations of peak and non-peak values in each year.
- Deleted:** the 30th and 920th
- Deleted:** the 540th and 830th
- Deleted:** are more
- Deleted:** threats



844

845 Figure 3. Comparisons of mean 10-fold CV RMSEs among different regression models with various sizes of predictors subsets. The
 846 response variable in (b) binomial GLM and (a) other models is hypoxia occurrence (hypoxia) and hypoxic area (HA), respectively.
 847 Note that the CV RMSEs of negative binomial GAM and Poisson GAM with the size of six are out of the range shown. CV RMSE
 848 curves of the Poisson GLM, negative binomial GLM, and quasi-Poisson GLM overlap, while those of Poisson GAM and quasi-
 849 Poisson GAM overlap when size < 5. The minimum size of predictor subsets is two since PEA and SOCalc are forced into every
 850 subset.



854
855 **Figure 4.** Comparisons of model predicted HA and ROMS-hindcast HA in the test set. RMSEs and R²s are derived between model
856 Bagging mean and ROMS-hindcast HA.

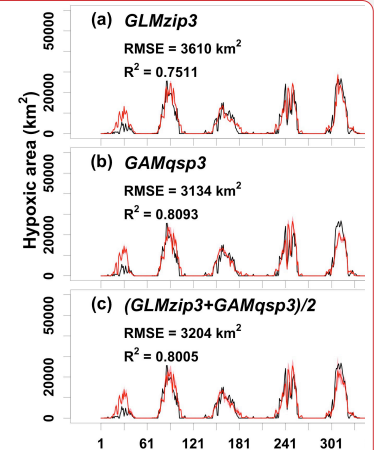
857 **Table 2** Mean absolute percentage bias between predicted and hindcast HA in the test set within different ranges of hindcast HA.
858 The mean bias when hindcast HA < 5,000 km² is not shown since the prediction accuracy at high HA ranges is a more important
859 feature of HA prediction models. The threshold of 5,000 km² is chosen because it is the goal HA set by the Action Plan (Mississippi
860 River/Gulf of Mexico Watershed Nutrient Task Force, 2001; 2008). HA above this threshold is more worthy of attention.

Hindcast HA range (km ²)	GLMzip3	GAMqsp3	Ensemble
[5000, 10000]	38	40	36
[10000, 20000]	32	25	28
[20000, 30000]	34	26	28
≥ 30000	29	28	25
Average	33	30	29

861

862 3.2.3 Model interpretation for GLMzip3

863 We applied the complete ROMS training set to the model construction of GLMzip3. Coefficients for PEA, SOCal_t, and
864 DCP_{Temp} (Table 3) are all found significantly positive ($p < 0.001$) in the count model, while coefficients for these predictors are
865 significantly negative ($p < 0.001$) in the zero-excess model. The count model simulates the HA while the zero-excess model



Deleted:

Deleted: and found

Deleted: the c

Deleted: 2

870 estimates the probability of HA being zero. Higher PEA is consistent with stronger water stratification, while higher SOCalt
 871 and DCP_{Temp} are both corresponding to higher sediment oxygen consumption. Therefore, there is no surprise that higher PEA,
 872 SOCalt, and DCO_{Temp} are related to greater HA and higher hypoxia occurrence or lower probability of HA being zero. Results
 873 indicate that the GLMzip3 essentially builds up reasonable relationships between the response and predictors variables with a
 874 high agreement with physical and biochemical mechanisms. Since the ranges of normalized predictors are from 0 to 1,
 875 comparisons of regression coefficients indicate that effects of PEA (2.8037 in the count model and -10.4439 in the zero-excess
 876 model, same hereafter) are considered more important than SOCalt (0.9057 and -7.3100) and DCP_{Temp} (0.8425 and -95698).
 877 The result is consistent with the findings of previous studies which emphasized that the physical impacts are stronger than the
 878 biological impacts on HA estimates (Yu et al., 2015; Mattern et al., 2013).

879 **Table 3. Regression coefficients of GLMzip3.**

Count model coefficients (Poisson with log link):				Zero-excess model coefficients (binomial with logit link):					
	Estimate	Std. Error	z value	Pr (> z)		Estimate	Std. Error	z value	Pr (> z)
Intercept	3.6397	0.0017	2120.5	<2E-16***	Intercept	7.7641	0.2761	28.12	<2E-16***
PEA	2.8037	0.0014	1984.6	<2E-16***	PEA	-10.4439	0.6794	-15.37	<2E-16***
SOCalt	0.9057	0.0014	639.6	<2E-16***	SOCalt	-7.3100	0.5714	-12.79	<2E-16***
DCP _{Temp}	0.8425	0.0029	287.7	<2E-16***	DCP _{Temp}	-95698	0.4611	-20.75	<2E-16***
Significance	0 (***)			0.001 (**)	0.01 (*)				

codes:
 Log-likelihood: -2.675E6 on 8 degrees of freedom

Deleted: both
 Moved down [3]: (Yu et al., 2015; Mattern et al., 2013)
 Deleted: by
 Deleted: of the shelf hypoxia (Yu et al., 2015; Mattern et al., 2013) emphasizing
 Moved (insertion) [3]
 Deleted: 2

Deleted: 1.9897
 Deleted: 0021
 Deleted: 948.2
 Deleted: 9.1993
 Deleted: 3181
 Deleted: 9
 Deleted: 6763
 Deleted: 0016
 Deleted: 1681.4
 Deleted: 5986
 Deleted: 16.9
 Deleted: 0945
 Deleted: 9228
 Deleted: 663
 Deleted: 5508
 Deleted: 15.9
 Deleted: 8.7784
 Deleted: 3.5940
 Deleted: 0031
 Deleted: 1168.2
 Deleted: 4346
 Deleted: 21.9
 Deleted: 4939
 Deleted: 4E6

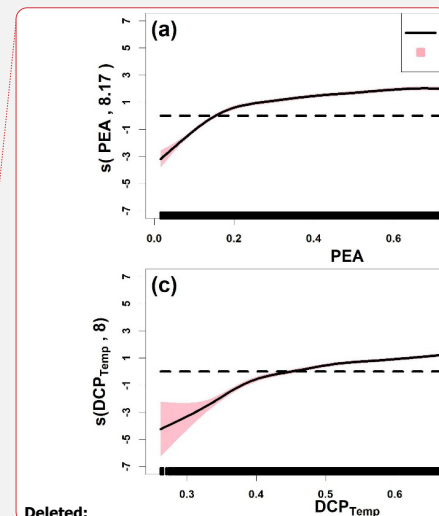
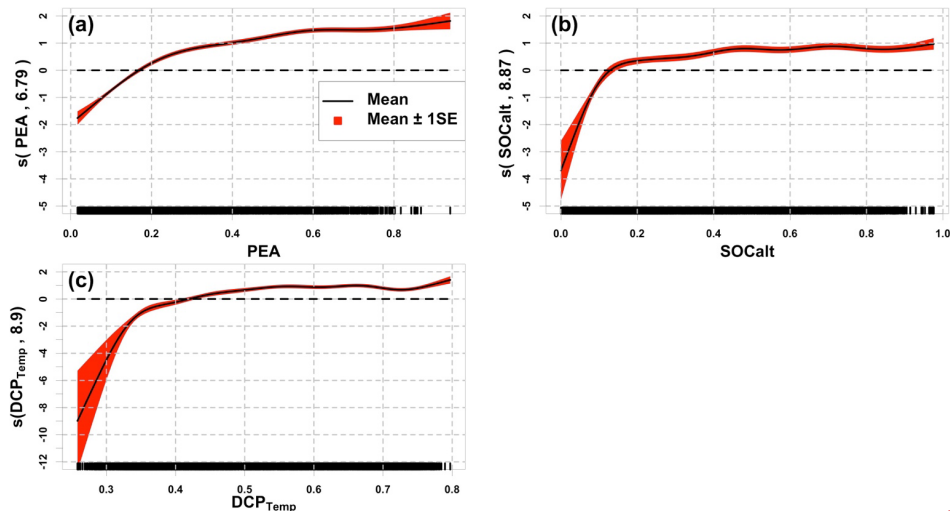
880

911 **3.3 Generalized additive models (GAMs) and the ensemble model**

912 GAMs are explored with an expectation of improving prediction performance in HA peaks by introducing non-parametric
913 effects of predictors. Using function “gam” in R package “mgcv” (version 1.8-36; Wood, 2011) with smooth functions as pure
914 thin plate regression splines (degree of freedom=9; Wood, 2003), three GAMs are studied and compared, i.e., Poisson GAM,
915 quasi-Poisson GAM, and negative binomial GAM. Following the same procedure, in GLM exploration, the best subset
916 searching approach is applied to the GAMs first. Although mean 10-fold CV RMSEs for the Poisson and quasi-Poisson GAMs
917 (Figure 3a) exhibit insignificant differences at sizes from two to five, the CV RMSEs for the former increase dramatically at a
918 size of six, which indicates that the model stability decreases with sizes. The negative binomial GAM has the greatest mean
919 CV RMSEs among the GAMs studied and has an extremely high mean CV RMSE at the size of six. The quasi-Poisson GAM
920 is considered the best GAM among the three. Although the mean CV RMSEs for the quasi-Poisson GAM reach the lowest at
921 the size of six, the best size is considered as three (including PEA, SOCalt, and DCP_{Temp}) at which CV RMSEs exhibit the
922 most saline decline, and beyond which mean CV RMSEs stabilize around 3,200 km². The quasi-Poisson GAM with three
923 predictors involved is symbolized as GAMqsp3.

924
925 Component plots of the GAMqsp3 (Figure 5) imply that HA generally increases as the chosen predictors increase. Note that
926 the summation of all smooth function terms contributes directly to the log of fitted HA. Such results agree with those found
927 by model GLMzip3. However, the component plots provide more detailed information about the rate of changes in HA. The
928 effective degrees of freedom range from 6.79 to 8.90, indicating strong non-linear effects of the predictors on the variability of
929 HA. The HA is more sensitive to the predictors in the low-value ranges but becomes nearly stable in the medium- and high-
930 value ranges of predictors. This implies that bottom hypoxia develops rapidly in early summer when water stratification and
931 sediment oxygen demand start to increase. On the other hand, the smooth functions of SOCalt and DCP_{Temp} have a sharper
932 slope than that of PEA at the low-value range. It suggests that at the first stage of hypoxia development in late spring and early
933 summer, sedimentary biochemical processes contribute more than water stratification. The bottom hypoxic water further
934 extends with a much lower expansion speed as the stratification and SOCalt further intensify. Nevertheless, the smooth function
935 of PEA is slightly greater also with a more acute slope than those found for SOCalt and DCP_{Temp} in the medium- and high-
936 value regimes of the predictors. It indicates that the HA variability is more related to the hydrodynamic changes in the shelf
937 than the biochemical effects during mid-summers. The result is consistent with the findings by Yu et al., (2015) and Mattern
938 et al. (2013). The GAMqsp3 model provides reasonable interpretations on the hypoxic area mechanisms.

- Deleted: "
- Deleted: "
- Deleted: procedur
- Deleted: The
- Deleted: and are the lowest among those
- Moved (insertion) [1]
- Deleted: all GLMs and GAMs studied.
- Deleted: these two types of GAMs both
- Deleted: five
- Deleted: considering
- Deleted: exhibits
- Moved up [1]: The negative binomial GAM has the greatest mean CV RMSEs among the GAMs studied and has an extremely high mean CV RMSE at the size of six.
- Deleted: It is, therefore, dropped out of the list of candidate models. ...
- Deleted: (
- Deleted:) is chosen as the best GAM since it relaxes the mean-variance equality assumption which should not be applied to the HA dataset due to the overdispersion issue
- Deleted: model
- Deleted: The smooth functions of PEA and DCP_{Temp} are considerably greater than the smooth function of SOCalt indicating that the contributions of the former two predictors are greater than the effect of SOCalt on the daily variability of HA.
- Deleted: fitted HA equals the
- Deleted: .
- Deleted: of
- Deleted: 8
- Deleted: 54
- Deleted: changes
- Deleted: It
- Deleted: SOC
- Deleted: previous studies of the shelf hypoxia (Yu et al., 2015; Mattern et al. 2013) emphasizing that the physical impacts are stronger than the biological impacts on HA estimates.
- Deleted: A short conclusion is made that the



Deleted:

Deleted: pink

Deleted: Note that the predictors shown have been normalized.

Deleted: 134

Deleted: 8093

Deleted: 8

Deleted: , suggesting

Deleted: produce underestimated predictions

Deleted: HA

Deleted: (like peaks

Deleted: the 310th and 920th

Deleted: since there is no clue showing the apparent superiority of either model in HA peak predictions. We

Deleted: i

Deleted: 204

Deleted: 8005

Deleted: the 310th and 920th

975

976 Figure 5. Component plots of model GAMqsp3. Solid black lines represent the mean of the smooth function, while the red area
977 denotes the range of mean \pm 1SE. Numbers in brackets represent effective degrees of freedom for the corresponding smooth terms.
978 Black bars at the x axis indicate the density of corresponding normalized predictors. Dashed black lines are straight lines of zero
979 along the predictor domains.

980 The prediction performance of GAMqsp3 is estimated using the Bagging ensemble method (Figure 4b). The RMSE and R^2
981 between the Bagging mean and ROMS-hindcast HA is 3,157 km² and 0.7858, respectively. They are 13 % lower and 9 %
982 higher than the corresponding statistics found for the GLMzip3, respectively. MAPB between GAMqsp3 predicted and
983 hindcast HA ranges from 25 % to 40 % with an average of 30 % (Table 2). Such statistics are generally lower than those found
984 in GLMzip3. Results suggest that GAMqsp3 outcompetes GLMzip3 in terms of overall performance. However, GAMqsp3
985 tends to underestimate HA peaks (like those seen at peaks around samples 750 and 901) some of which are overestimated by
986 the GLMzip3. Therefore, instead of determining the best model out of the two, ensemble HA predictions blending efforts of
987 both GLMzip3 and GAMqsp3 are carried out with an expectation to improve model performance in the peak forecast. We
988 assumed that the contributions of GLMzip3 and GAMqsp3 are equally weighted and, thus averaged the predicted HA by
989 GLMzip3 and GAMqsp3 and calculated the 95 % PIs given the Bagging results of these models (Figure 4c). As expected, the
990 overall performance of the ensemble forecast is somewhere between the performance of GLMzip3 and GAMqsp3 with an
991 RMSE of 3,256 km² and an R^2 of 0.7721. However, some HA peak events (like peaks around samples 750 and 901) which are
992 overestimated by GLMzip3 but are underestimated by GAMqsp3 are accurately predicted by the ensemble approach. MAPB
993 also indicates an increase in peak prediction performance by the ensemble model. The statistic is within a range of 25 % to 36
994 % with an average of 29 %. At extreme peaks (hindcast HA \geq 30,000 km²), compared to the MAPB by GLMzip3 (29 %) and

1012 by GAMqsp3 (28 %), the statistic decreases to 25 % by the ensemble model. The ensemble model provides a higher accuracy
1013 in peak forecast given minor sacrifices in overall performance.

1014 3.4 Application to Global Forecast Products (HYCOM)

1015 The power of the prediction model relies on the availability of the forecast of predictors. In this section, we discuss the model's
1016 transferability using an independent global ocean product. The Global Ocean Forecasting System (GOFS) 3.1 provides global
1017 daily analysis products and an eight-day forecast in a daily interval with a horizontal resolution of 1/12 °. The products
1018 (hereafter referred to as HYCOM-derived products) are derived by a 41-layer HYCOM global model (Bleck and Boudra, 1981;
1019 Bleck, 2002) with data assimilated via the Navy Coupled Ocean Data Assimilation (NCODA) system (Cummings, 2005;
1020 Cummings and Smedstad, 2013). The Mississippi River total nitrate+nitrite loadings are provided by USGS NWIS as described
1021 in section 2.1.2. Daily HYCOM-derived hydrodynamics and USGS river nitrogen loads from 1 January 2007 to 26 August
1022 2020 are used to reconstruct predictors of PEA, SOCalt, and DCP_{Temp}. Relationships of ROMS-derived and HYCOM-derived
1023 predictors are examined in Figure 6. The magnitudes of HYCOM-derived SOCalt and DCP_{Temp} match up with the
1024 corresponding ROMS-derived predictors, respectively, although HYCOM-derived predictors are found slightly greater.
1025 Simple linear regression for these predictors illustrates that the linear relationships between the ROMS and HYCOM products
1026 are significant with the R² ranging from 0.94 to 0.96. The intercept terms are at least one-order smaller than the magnitudes of
1027 corresponding predictors. Therefore, the HYCOM global products are deemed to agree with the ROMS hindcasts for SOCalt
1028 and DCP_{Temp}. Nevertheless, the magnitude of HYCOM-derived PEA is found much lower than the ROMS-derived PEA
1029 (Figure 6a). Simple linear regression indicates a significant linear relationship between the natural log transformation of PEA
1030 from the two datasets (R²=0.66).

1031
1032 At land-sea interfaces, the HYCOM global model is forced by monthly riverine discharges, which weaken the model
1033 performance in coastal regions. The hydrodynamics in the LaTex Shelf is highly affected by the freshwater and momentum
1034 from the Mississippi and the Atchafalaya Rivers. Monthly river forcings in HYCOM are essentially weaker than daily forcings
1035 used in our ROMS setups and can result in a less stratified water column (i.e., lower PEA). Therefore, it is necessary to scale
1036 the magnitude of HYCOM-derived PEA to that of the ROMS hindcast. It can be achieved by using the natural log
1037 transformation and simple linear regression as discussed. We then adjusted HYCOM-derived PEA but kept the HYCOM-
1038 derived SOCalt and DCP_{Temp} unchanged before the application of the ensemble model.

1039
1040 The Bagging approach is implemented again to assess the performances of the ensemble model. During each iteration
1041 (N=1,000), the GLMzip3 and GAMqsp3 are trained using the ROMS training set and then applied to the adjusted HYCOM-
1042 derived predictors for HA prediction from 1 January 2012, to 26 August 2020 (Figure 7a). The ensemble method provides
1043 averages and 95 % PIs of predicted HA blending Bagging results by GLMzip3 and GAMqsp3. Compared to observed HA by
1044 mid-summer Shelf-wide cruises, the ensemble model fails in the summers of 2013, 2014, 2017, and 2018, but provides accurate

Deleted: HYCOM

Deleted: Dataset

Deleted: 4 Discussion ¶
A promising HA forecast is provided by the ensemble model with a low RMSE (3,204 km²), a high R² (0.8005), and a precise performance in capturing hypoxic area peaks in the summers.

Deleted: '

Deleted: ¶

Deleted: . (GLBy0.08 expt_93.0, available via Error! Hyperlink

Deleted:)

Deleted: the

Deleted: as

Deleted: Daily data

Deleted: retrieved and are

Deleted: studied. Predictors

Deleted: are reconstructed using HYCOM-derived variables and Mississippi River daily total nitrate and nitrite loadings downloaded from the USGS NWIS.

Deleted: 93

Deleted: 95

Deleted: 69

Deleted: s

Deleted: set up

Deleted: 2019

Deleted: .

Deleted: i

Deleted: the ROMS-hindcast

Deleted: performs an overall accurate HA forecast with an RMSE and an R² of 4,571 km² and 0.8178, respectively (Figure 7). The HA peaks

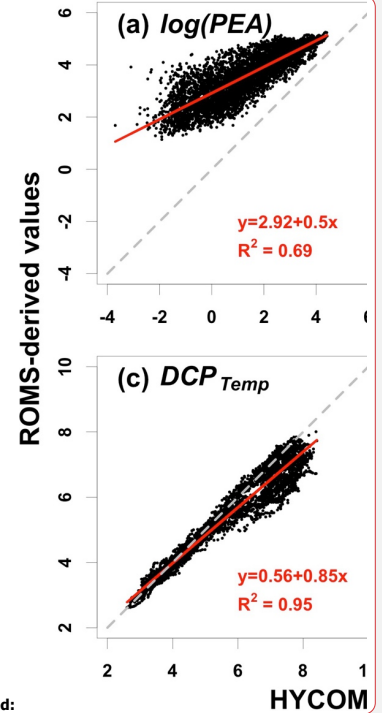
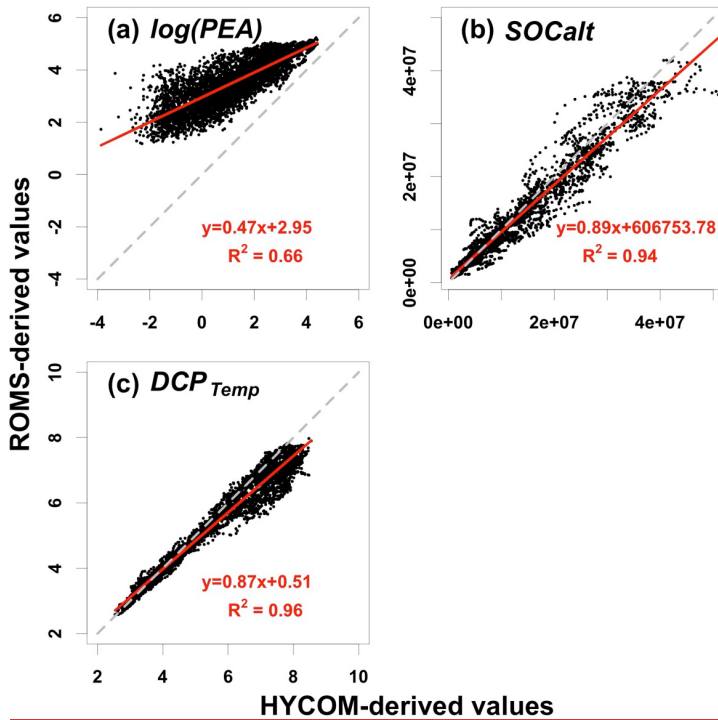
Deleted: both 2019 and 2020

1078 predictions in other summers. The width of 95 % PI is larger during high HA periods suggesting less stability in the HA peak
 1079 forecast. The overall performance is barely acceptable with an R^2 of 0.4242, an RMSE of 5,088 km², and a SI of 38%. The
 1080 bias against the observations can be ascribed to the HYCOM's failures in reproducing the shelf hydrodynamics, although
 1081 HYCOM-derived predictors are adjusted before being applied to the model (Figure 6a). We noticed that among the three
 1082 variables, HYCOM-derived PEA exhibits the largest deviation from that generated by ROMS. We then applied the model
 1083 using ROMS-derived PEA, HYCOM-derived SOCalt, and HYCOM-derived DCP_{Temp} (Figure 7b). The performance of the
 1084 ensemble model was largely enhanced with a higher R^2 (0.9255), a much lower RMSE (3,751 km²), and a lower SI (28%)
 1085 compared to that using pure HYCOM products. These results indicate that the ensemble model can produce a highly accurate
 1086 prediction for HA summer peaks once water stratification is well resolved. Instead of using monthly river forcings, the
 1087 HYCOM model may possibly resolve the shelf hydrodynamics by utilizing daily river discharges of the Mississippi and the
 1088 Atchafalaya Rivers.

Deleted: are well captured by the model with slight underestimates at the first peak and slight overestimates at the second.

Deleted: derived ... scribed from ... o the HYCOM's failures in reproducing the shelf hydrodynamics, although even though adjustments to the ... YCOM-derived predictors are implemented ... djusted before being applied to the model (Figure 6a). Model sensitivity to hydrodynamics is thus studied. ... e noticed that among the three variables, HYCOM-derived PEA exhibits the largest deviation from that generated by ROMS. The prediction model is then applied to the HA prediction using ... e then applied the model using predictors of ... OMS-derived PEA, HYCOM-derived SOCalt, and HYCOM-derived DCP_{Temp} (Figure 7b). The performance of the ensemble model almost captures all HA peaks shown (Figure 7b) and provides great overall performance with a much greater ... as largely enhanced with a higher R^2 (0.9255), a much lower RMSE (3,751 km²), and a lower SI (28%) compared to the performances ... hat using pure HYCOM products. These indicate that the ensemble model can produce a high accuracy in HA predictions ... highly accurate prediction for HA at ... umm ... [24]

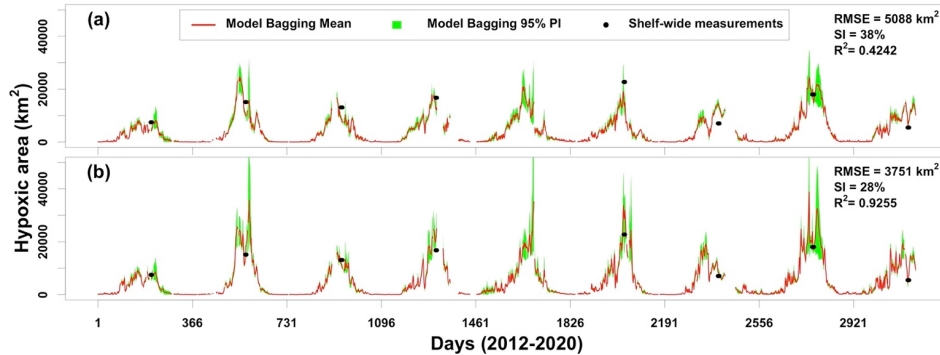
Deleted: would be further improved.



Deleted:

1089

1242 Figure 6. Scatter plots of (a) $\log(\text{PEA})$ (unit: $\log(\text{J m}^{-3})$), (b) SOCalt (unit: mmol s^{-1}), and (c) DCP_{Temp} (unit: 1) between ROMS
 1243 and HYCOM simulations. Note that the solid red lines represent linear regression lines, while the dashed grey lines are diagonals
 1244 with a slope of 1 and an intercept of 0. Daily data compared are from 2007 to 2020.

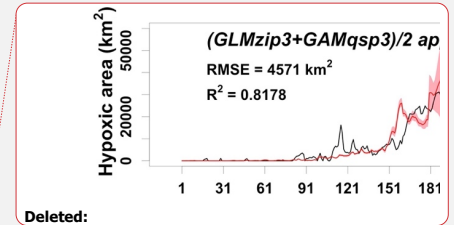


1246 Figure 7. Comparisons of daily predicted HA by ensemble model ((GLMzip3+GAMqsp3)/2) when applied to adjusted HYCOM
 1247 products and Shelf-wide measurements from 2012 to 2020. Model results shown in (a) are predicted using pure HYCOM-derived
 1248 products (i.e., PEA, SOCalt, and DCP_{Temp}), while those in (b) are predicted by ROMS-derived PEA, HYCOM-derived SOCalt, and
 1249 HYCOM-derived DCP_{Temp} . Discontinuity of the predictions is due to the lack of riverine nitrate+nitrite records at site USGS
 1250 07374000 in the Mississippi River.

1251 4 Discussion

1252 4.1 Model performance evaluation

1253 To further assess the robustness of our model, we reviewed a suite of existing forecast models that are transitioned operationally
 1254 (in early June) to the NOAA ensemble forecast for each summer. (data sources are listed in Table 4). Using the ROMS-derived
 1255 predictors, daily HA predictions during the Shelf-wide cruises periods are averaged for each summer from 2012 to 2020 and
 1256 are compared to the cruise observations. As shown in Figure 8a, our model predictions fit well with the Shelf-wide observation
 1257 for summers with or without strong windy events prior to the cruises. Other seasonal forecast models have similar performances
 1258 to our model in fair-weather summers (i.e., 2012, 2014, 2015, and 2017) but fail to produce an accurate forecast for several
 1259 summers with strong wind conditions (i.e., 2018 and 2020). Percentage differences between predictions and observations
 1260 (Figure 8b) also emphasize the superiority of our model with the percentages ranging from -24 % to 7 % for fair-weather
 1261 summers and from 7 % to 35 % for summers with strong wind or storms. All models underestimate or overestimate observed
 1262 HA in fair weather summers, but overestimate HA in windy summers. Our model provides the most accurate overall
 1263 performance with the highest R^2 (0.9200, $N=8$), the lowest RMSE ($2,005 \text{ km}^2$, $N=8$), the lowest SI (15 %, $N=8$), and the lowest
 1264 MAPB (18 %, $N=8$) among all models (Table 4). The multiple linear regression model developed by Forrest et al. (2011)
 1265 provides the second optimal prediction. For fair-weather summers, the NOAA ensemble predictions produce the best



Deleted:

Deleted: Daily time series

Deleted: ROMS-hindcast HA

Deleted: 2019

Deleted: Comparisons to other seasonal

Deleted: forecast models

Deleted: W

Deleted: multiple prevailing HA seasonal forecast models which are

Deleted: NOAA-sponsored

Deleted: and have been

Deleted:

Deleted: .

Deleted: D

Deleted: no matter

Deleted: to

Deleted: some

Deleted: More s

Deleted: statistics (Table 4) show that o

285 estimation of the observed HA with a MAPB of 9 % (N=4), while our model results rank the second (15 %, N=4). However,
286 our model performs the best in windy summers with a MAPB of 18 % (N=4), while other models produce a MAPB from 33 %
287 to 74 %.

288
289 Models developed by Turner et al. (2006, 2008, 2012) and Laurent and Fennel (2019) are calibrated on May nitrate or
290 nitrate+nitrite loads from the Mississippi–Atchafalaya River Basin, assuming that the predicted HA in summers are under fair
291 weather. It is expected that models excluding wind effects can hardly produce accurate forecasts during summers with strong
292 winds or storms. Wind mixing effects on HA are considered in reaeration by introducing a wind stress term in the mechanistic
293 model (Obenour et al., 2015), while in the Bayesian model by Scavia et al. (2013), the wind effects are considered indirectly
294 via an estimation based on current velocity and the reaeration rate given different wind conditions (i.e., fair weather, strong
295 westerly winds, and storms). However, as shown in Figure 1a, PEA_{wind} , which can also be interpreted as wind power, is found
296 poorly correlated to daily HA ($R=-0.2458$) compared to other highly correlated predictors and is dropped out of the candidate
297 list by the best subset searching approach. Forrest et al., (2011) also found that monthly wind power is not significantly
298 correlated to summer HA due to the short timescales of strong wind events. Therefore, the wind mixing effects considered by
299 Obenour et al. (2015) and Scavia et al. (2013) have limited contribution to the prediction of the interannual variability of the
300 HA. Indeed, our model construction process indicates that wind mixing, freshwater plume, and water temperature jointly
301 control the water stratification and vertical mixing, which directly modulates the reoxygenation of shelf water. PEA can serve
302 better in representing such effects rather than by wind speed or wind power alone. The daily PEA is significantly correlated to
303 daily HA ($R=0.8178$, $p<0.01$; Figure 1a) while the nonlinear effects of PEA cannot be neglected (Figure 5a). Therefore, an
304 accurate forecast of shelf hydrodynamics is critical for a robust summer HA prediction.

Deleted: The Bayesian model (Scavia et al., 2013), the multilinear regression model (Forrest et al., 2011), and the mechanistic model (Obenour et al., 2015) take into account weather impacts on the HA by adding June–July wind speeds or wind stress besides riverine May nitrate or nitrate+nitrite loads into the models. There is no surprise that models excluding wind effects hardly produce accurate forecasts during summers with strong winds or storms. Nevertheless, models exhibit poorly under strong mixing events even though weather impacts are considered.

Deleted: 's.

Deleted: Bayesian model

Deleted: by different

Deleted: prescribed distributions of the downstream

Deleted:

Deleted: in

Deleted: 's.

Deleted: 's.

Deleted: models

Deleted: HA

Deleted: It is the combined effects of the

Deleted: winds

Deleted: that

Deleted: contribute directly to the

Deleted: or

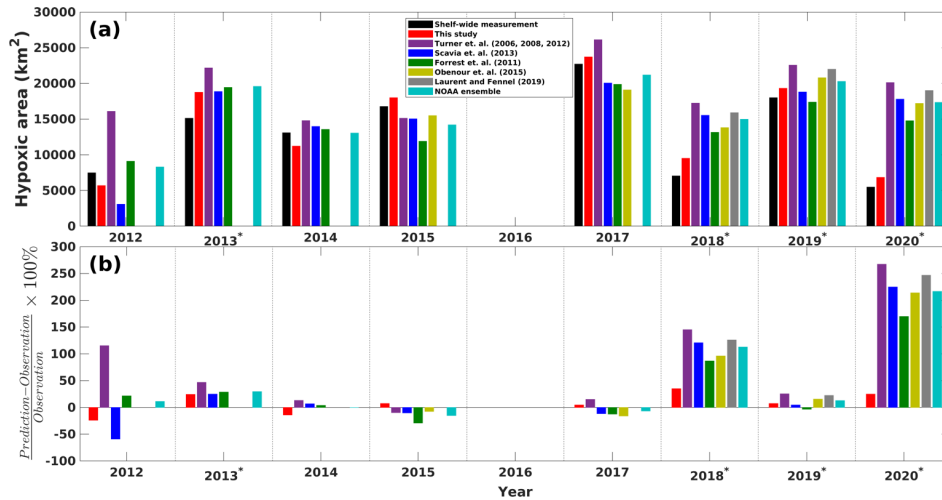
Deleted:

Deleted: A state variable of

Deleted: Indeed, d

Deleted: , while the

Deleted: accurate



1334

1335 **Figure 8. (a)** Comparisons of Shelf-wide measured and the best estimates of model predicted HA during the Shelf-wide cruise
 1336 periods. **(b)** Percentage differences between different model predictions and Shelf-wide measurements. The superscript asterisks
 1337 indicate high-wind years prior to the cruises.

1338

1339 **Table 4** Statistics comparisons between model predictions and the Shelf-wide measurements. The R^2 's for predictions by Obenour et
 1340 al. (2015) and Laurent and Fennel (2019) are not given since the numbers of available records are small (N=5 and 3, respectively).
 1341 Numbers in parentheses indicate the numbers of compared records. Underscript "fair" and "windy" indicate that averages of
 1342 corresponding statistics are conducted for fair-weather and windy summers, respectively.

	This study	Turner et al. (2006, 2008, 2012)	Scavia et al. (2013)	Forrest et al. (2011)	Obenour et al. (2015)	Laurent and Fennel (2019)	NOAA ensemble
R^2	0.9200 (N=8)	0.3017 (N=8)	0.2577 (N=8)	0.4061 (N=8)	– (N=5)	– (N=3)	0.3566 (N=8)
RMSE (km)	2005 (N=8)	7750 (N=8)	5797 (N=8)	4710 (N=8)	6412 (N=5)	9614 (N=3)	5460 (N=8)
SI	15 % (N=8)	59 % (N=8)	44 % (N=8)	36 % (N=8)	46 % (N=5)	95 % (N=3)	41 % (N=8)

MAPB	18 % (N=8)	80 % (N=8)	58 % (N=8)	44 % (N=8)	70 % (N=5)	132 % (N=3)	51 % (N=8)
MAPB _{fair-weather}	15 % (N=4)	46 % (N=4)	25 % (N=4)	18 % (N=4)	8 % (N=2)	– (N=0)	9 % (N=4)
MAPB _{windy}	18 % (N=4)	58 % (N=4)	40 % (N=4)	33 % (N=4)2	43 % (N=3)	74 % (N=3)	40 % (N=4)
Data source (access in June 2022)	https://gulfhypoxia.net/ (Turner et al., 2006; 2008; 2012) http://scavia.seas.umich.edu/hypoxia-forecasts/ (Scavia et al., 2013) https://www.vims.edu/research/topics/dead_zones/forecasts/gom/index.php (Forrest et al., 2011) https://obenour.wordpress.ncsu.edu/news/ (Obenour et al., 2015) https://memg.ocean.dal.ca/news/ (Laurent and Fennel, 2019), https://www.noaa.gov/news (NOAA ensemble).						

1343

1344 **4.2 Task force nutrient reduction.**

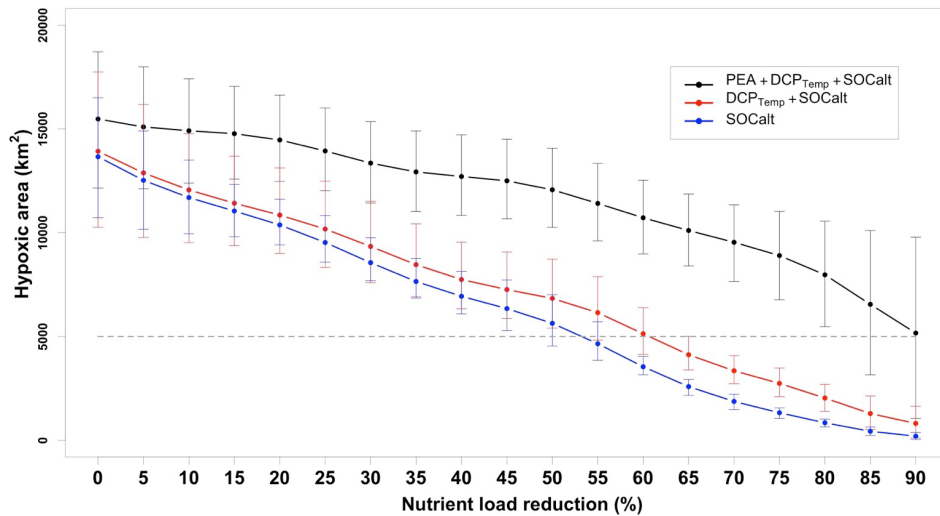
1345 [In this section we assess the effects of nutrient reductions on HA using our model. Since 2001, the Mississippi River/Gulf of](#)
1346 [Mexico Hypoxia Task Force has set up a goal of controlling the size of mid-summer hypoxic zone below 5,000 km² in a 5-](#)
1347 [year running average \(Mississippi River/Gulf of Mexico Watershed Nutrient Task Force, 2001; 2008\) by reducing riverine](#)
1348 [nutrient loads. Because the monthly riverine silicate, phosphate, and nitrate+nitrite loads are highly correlated \(Table A1\), here](#)
1349 [we refer to nitrogen load \(the only nutrient that has daily measurements\) as the proxy for all riverine nutrients. The averaged](#)
1350 [summer HA during the Shelf-wide cruises in the most recent five years \(2015, 2107, 2018, 2019, and 2020\) are calculated](#)
1351 [with different nutrient reduction scenarios, and are shown in Figure 9. The PEA, bottom temperature, and river discharges are](#)
1352 [unchanged, while the SOCal_t is altered by reducing the nutrient concentration from 5% to 90%. The averaged observed HA is](#)
1353 [14,000 km², while the averaged prediction by our ensemble model is 15,478 km², which is 11 % greater than the observation.](#)
1354 [As a leading time of 44 days \(Figure A3a\) is prescribed in SOCal_t prior to Shelf-wide summer cruises in mid-late July,](#)
1355 [reduction strategies are applied to mid-June nutrient loads rather than May loads in our model. The monthly averaged total](#)
1356 [nitrogen loads for the 1980–1996 summers \(April, May, and June\) are \$1.96 \times 10^8\$ kg/month \(Battaglin et al., 2010\). It is](#)
1357 [comparable to the June-mean total nitrogen load \(\$1.6 \times 10^8\$ kg month⁻¹\) for the 2015–2020 period. We find that a 92 %](#)
1358 [reduction, which corresponds to a total nitrogen load of \$5.5 \times 10^5\$ kg day⁻¹ or \$1.6 \times 10^7\$ kg month⁻¹, is needed for the mid-June](#)
1359 [nutrient loads to achieve the goal of a 5,000 km² HA.](#)

1359

- Deleted: <https://gulfhypoxia>
- Deleted: <http://scavia>
- Deleted: <https://www>
- Deleted: <https://obenour>
- Deleted: <https://memg>
- Deleted: <https://www>
- Deleted:
- Deleted: [Link needed be fixed to entire website address](#)
- Deleted: Scenario projections
- 4.2.1 Nutrient reduction strategy
- Deleted: controlling
- Deleted: the
- Deleted: Effects of nutrient reductions on HA can be estimated by our forecast model. The nutrient reductions should be interpreted as multi-nutrient reductions as
- Deleted: .
- Deleted: given
- Deleted: in
- Deleted: (
- Deleted:)
- Deleted: kept
- Deleted: changing
- Deleted: only
- Deleted: (2015–2020, except 2016)
- Deleted: We decreased daily nutrient concentrations referring to the loads on the corresponding days. Since a
- Deleted: introduced
- Deleted: prescribed
- Deleted: the
- Moved (insertion) [2]
- Deleted: to
- Deleted: To achieve the HA reduction goal of 5,000 km² for the 2015–2020 mean (except 2016; Figure 9),
- Deleted: 0
- Deleted:
- Deleted: required for
- Moved up [2]: The monthly averaged total nitrogen loads for the 1980–1996 summers (April, May, and June) are 1.96×10^8 kg/month (Battaglin et al., 2010). It is comparable to the June-mean total nitrogen load (1.6×10^8 kg month⁻¹) for the 2015–2020 period.
- Deleted: It corresponds to a rate of total nitrogen load of 5.5×10^5 kg day⁻¹ or 1.6×10^7 kg month⁻¹. [25]
- Deleted: Our model suggests that a 92 % reduction in nutr... [26]

408

409 The recommended reduction strategy by our model is much more demanding than that by other models (Scavia et al., 2013;
 410 Obenour et al., 2015; Turner et al., 2012; Laurent and Fennel, 2019), which recommend a load reduction of 52%–58% related
 411 to the 1980–1996 average (Scavia et al., 2017). A recommendation of 92% reduction is closed to that by Forrest et al. (2011)
 412 (80%) when the coastal westerlies from 15 June to 15 July were considered in their regression model. Since water stratification
 413 is attributed to not only wind mixing effects but also effects from other physical processes (e.g., riverine freshwater transports
 414 and surface heating), models developed based solely on May nutrient loads (Turner et al., 2012; Laurent and Fennel, 2019) or
 415 nutrient loads and wind mixing (Scavia et al., 2013; Obenour et al., 2015) fail to capture water stratification’s contribution to
 416 hypoxia development. If a model considers the variability of HA to rely highly on the nutrient loads, then a moderate decrease
 417 in nutrient loads would result in a substantial HA reduction. For further illustration, we re-ran the model without consideration
 418 of the PEA (i.e., use DCP_{Temp} and SOCal_T or use only SOCal_T). Model results show a substantial shrink of HA with moderately
 419 reduced riverine nitrogen loads (Figure 9). In details, if only DCP_{Temp} and SOCal_T are used as the predictors, a nutrient reduction
 420 by 60% will satisfy the 5000 km² HA goal. And if we only use SOCal_T as the predictor, then a 55% reduction is sufficient.
 421 These results highlight the importance of considering PEA in HA predictions.



422

423 **Figure 9** 2015–2020 mean (except 2016) of predicted HA in scenarios of different nutrient load reduction strategies given different
 424 sets of predictors considered. Predictions by the ensemble model are conducted individually for the Shelf-wide cruise periods in
 425 different summers and averaged from 2015 to 2020. Horizontal bars indicate ranges of 95% PIs. Grey dashed lines represent the
 426 goal of 5,000 km² set by the Mississippi River/Gulf of Mexico Hypoxia Task Force. Note here nutrient reduction percentages are
 427 referred to mid-June nutrient loads in corresponding years.

Deleted: NOAA-supported ...odels (Scavia et al., 2013; Obenour et al., 2015; Turner et al., 2012; Laurent and Fennel, 2019), which recommend a load reduction of 52%–58% related to the 1980–1996 average (Scavia et al., 2017). However, o ... [27]

Deleted: 0

Deleted: ur estimate...is closed to that by Forrest et al. (2011) (80%) when who consider ...he coastal westerlies from 15 June to 15 July were considered in their regression model. Since water stratification is attributed to not only wind mixing effects but also effects from coastal current ... [28]

Deleted:

Deleted: syst

Deleted: xxx, xxx

Deleted: on the relationship between ...olely on May nutrient loads and HA ...Turner et al., 2012; Laurent and Fennel, 2019) and developed on...r both ...utrient loads and wind mixing (Scavia et al., 2013; Obenour et al., 2015) fail to represent...apture ...ater stratification’s contribution to hypoxia development well... If a model The...onsiders the variability of HA thus ...o rely highly on the nutrient loads, which...hen turns out that ... moderate decrease in nutrient loads would result in a great...ubstantial ...A reduction. For further illustration, we retained our model ... [29]

Deleted: un th...n e ... [30]

Deleted: using different sets of predictors...ithout consideration of the PEA (i.e., use DCP_{Temp}+...nd SOCal_T and ... [31]

Deleted:

Deleted: only.... To meet the hypoxia reduction goal, nutrient reduction percentages decrease drastically as predictors are removed from the model ... [32]

Deleted: s

Deleted: For the case with only...n details, if only DCP_{Temp} and SOCal_T are involved...sed as the predictors, a the ...utrient reduction percentage is...y 60% related to the corresponding mid-June loads...ill satisfy the 5000 km² HA goal,... And if we only use SOCal_T while percentage decrease to around...s the predictor, then a 55% if only SOCal_T is considered in the regression model...n reduction is sufficient. Note that only SOCal_T is related to nutrient loads while the other two are not...these results model ...ighlight the importance of involving...onsidering PEA for...n HA predictions. As the PEA, which can be reproduced and forecasted from the 3-dimensional water density simulations by ROMS, is taken into account, a part of HA variability is contributed by PEA variability. It results in a more nutrient reduction percentage to meet the HA goal of 5,000 km². ... [33]

566 5 Conclusion

567 In this study, we present a novel HA forecast model for the LaTex Shelf using statistical analysis. The model is trained using
568 numeric simulations from 1 January 2007 to 26 August 2020 by a 3-dimensional coupled hydrodynamic–biogeochemical
569 model (ROMS). Multiple GLMs (regular Poisson GLMs, quasi-Poisson GLMs, negative binomial GLMs, zero-inflated
570 Poisson GLMs, and zero-inflated negative binomial GLMs) and GAMs (regular Poisson GAMs, quasi-Poisson GAMs, and
571 regular negative binomial GAMs) are assessed for HA predictions. Comparisons of model prediction performance illustrate
572 that an ensemble model combining the prediction efforts of a zero-inflated Poisson GLM (GLMzip3) and a quasi-Poisson GAM
573 (GAMqsp3) provides the most accurate HA forecast with PEA, SOCal, and DCP_{Temp} as predictors. The ensemble model is
574 capable of explaining up to 77 % of the total variability of the hindcast HA and also provides a low RMSE of 3.256 km² and
575 low MAPBs for overall (29 %) and peak predictions (25 %) when compared to the daily ROMS hindcasts.

576
577 We then applied the hydrodynamics field generated by a global model (HYCOM, GOFS 3.1) and performed a HA hindcast
578 for the period from 1 January 2012 to 26 August 2020. The overall performance is barely acceptable with an R² of 0.4242, an
579 RMSE of 5.088 km², and a SI of 38 % against the Shelf-wide summer cruise observations, largely due to HYCOM's relatively
580 poor representation of shelf stratification. A substitution of ROMS-derived PEA led to a pronounced improvement with an R²
581 of 0.9255, an RMSE of 3.751 km², and an SI of 28 %.

582
583 The ensemble model also provides an efficient yet more robust summer HA forecast than existing HA forecast models.
584 Comparing against the Shelf-wide cruise observations, our model provides a high R² (0.9200 vs 0.2577–0.4061 by existing
585 forecast models, same comparison hereinafter), a low RMSE (2.005 km² vs 4.710–9.614 km²), a low SI (15 % vs 36 %–95 %),
586 low MAPBs for overall (18 % vs 44 %–132 %), fair-weather summers (15 % vs 8 %–46 %), and windy summers (18 % vs 33
587 %–74 %) predictions. Sensitivity tests are conducted and suggests that a 92 % reduction in riverine nutrients related to the
588 1980–1996 summer average is required to meet the goal of a 5,000 km² HA. These results highlight the importance of
589 considering PEA in HA prediction.

590
591 **Code/Data availability:** Model data is available at the LSU mass storage system and details are on the webpage of the Coupled
592 Ocean Modeling Group at LSU (<https://faculty.lsu.edu/zxue/>). Data requests can be sent to the corresponding author via this
593 webpage.

594
595 **Author contribution:** Bin Li and Z. George Xue designed the experiments and Yanda Ou carried them out. Yanda Ou
596 developed the model code and performed the simulations. Yanda Ou, Bin Li, and Z. George Xue prepared the manuscript.

597
598 **Competing interests:** The authors declare that they have no conflict of interest.

Deleted: 4.3 Model improvement

The HA variability is more related to the hydrodynamic changes in the shelf than the biochemical effects as indicated by both regression coefficients of GLMzip3 (Table 3) and component plots of GAMqsp3 (Figure 5). The finding is consistent with that by Yu et al. (2015) and Mattern et al. (2013). Thus, an accurate forecast of the shelf hydrodynamic environment is critical to HA prediction. Using global hydrodynamic products (like HYCOM) can lead to poor performance (Figure 7a) even though the ensemble model is well trained by simulations from regional models. Improvements are needed in shelf area for the global models like by using the daily river discharges as land-sea boundary forcings. Alternatively, shelf hydrodynamics can be predicted by regional models (like ROMS). ROMS simulations can achieve better than global products with lateral open boundary conditions forced by the HYCOM global products, the upper boundary forced by global atmospheric forecast (e.g., National Centers for Environmental Prediction Climate Forecast System), and the lateral land-sea boundary forced by daily river discharges updated daily by USGS. For a short-term (<1 month) prediction, we can simply assume the river discharges hold the same magnitude as in the preceding month or week. On...

Deleted: an ensemble... novel HA forecast model for the LaTex Shelf is developed using the state-of-the-art statistic programming language R...sing statistical analysis. The model is trained u...

Deleted:

Deleted: Before splitting data into a training set and a test set, we applied regional average over the LaTex Shelf and min-max normalization to the hindcast data.

Deleted: are

Deleted: involved in the GLM and GAM...s predictors. Statistically significant coefficients for the predictors (for the the GLMzip3) and component plots (for the GAMqsp3) agr...

Deleted: †

Deleted: The ensemble model is then migrated to the

Deleted: hydrodynamics...ydrodynamics field generated by a global moeel

Deleted: ...OFS 3.1 products based on HYCOM...s which provides an eight-day forecast of global hydrodynamics...a

Deleted: 1st, 2019...to 26 August 26th, ...020. The overall performanceprediction...is barely acceptablerobust when compared the ROMS simulations (2019–2020)...with an R² of 0.4242

Deleted: the poor...YCOM's relatively poor representation performance of...f shelf water...stratification by the HYCOM in the river-dominated shelf... A change

Deleted: substitiuon

Deleted: to ...OMS-derived PEA can ...ead... to a pronounced improvement in model predictions ...ith an (...²=...f 0.9255, an RMSE of E=...751 km², and an SI of =...8 %)

Deleted: existing...existing HA forecast models. Comparing against the Shelf-wide cruise observations, our model provides a high R² (0.9200 vs 0.2577–0.4061 by existing forecast models, sam

Deleted: HA peaks in 2019 and 2020, respectively. To our best knowledge, this ensemble model is the first model providing efficient yet accurate daily HA forecast for the LaTex Shelf

1933

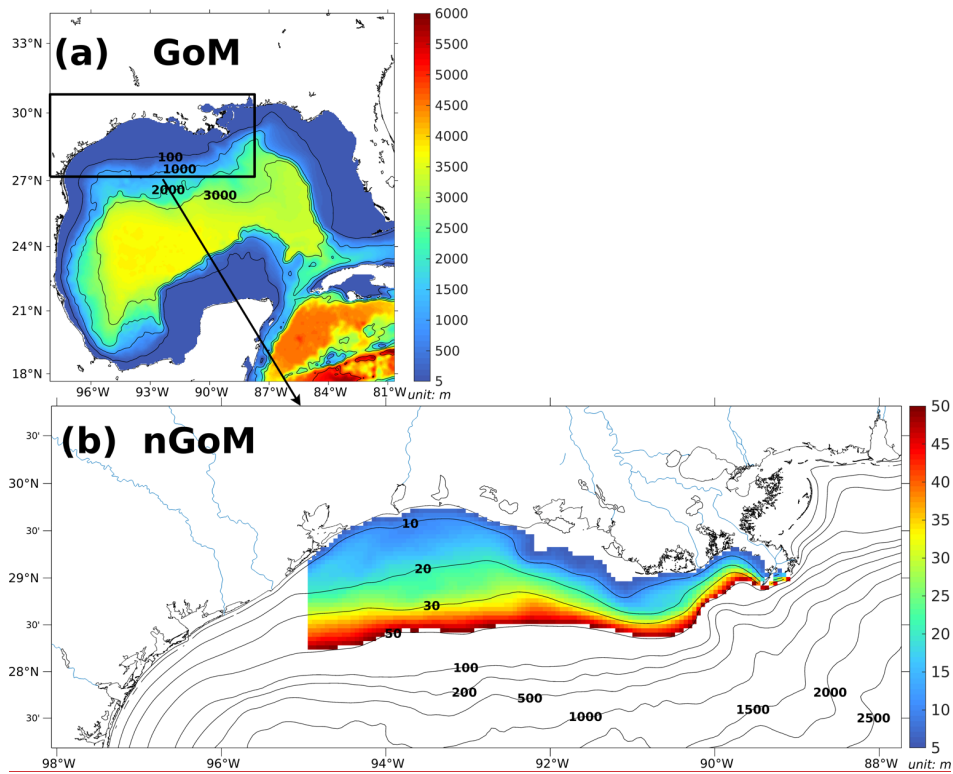
1934 **Acknowledgment:** Research support was provided through the Bureau of Ocean Energy Management (M17AC00019,
1935 M20AC10001). We thank Dr. Jerome Fiechter at UC Santa Cruz for sharing his NEMURO model codes. Computational
1936 support was provided by the High-Performance Computing Facility (clusters SuperMIC and QueenBee3) at Louisiana State
1937 University.

1938

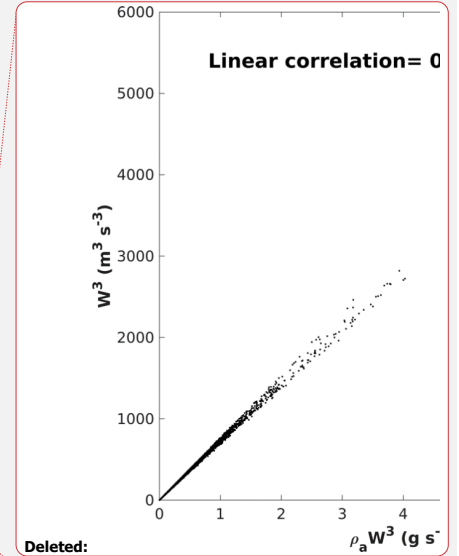
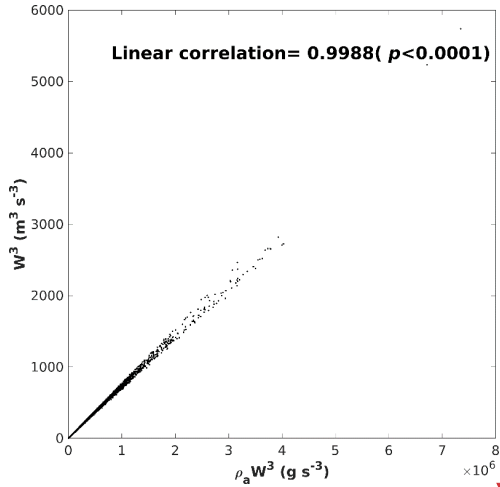
1939

Deleted:

1941 Appendix A:



1942
1943 Figure A1 (a) Bathymetry of the entire domain of the Gulf-COAWST described in the accompanying study (Part I) and (b) zoom-
1944 in bathymetry plot of the northern Gulf of Mexico (nGoM). The range of bathymetry of the color shaded area in (b) is from 6 to 50
1945 m, over which the regional averages of parameters are conducted.



Deleted:

Deleted: A1

Deleted: and

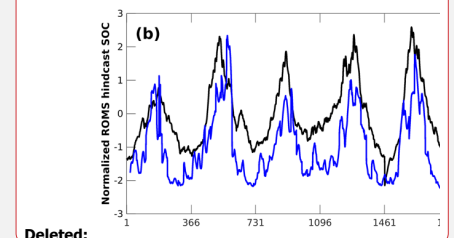
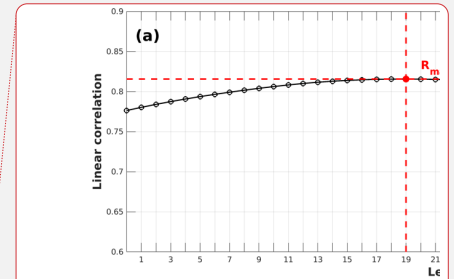
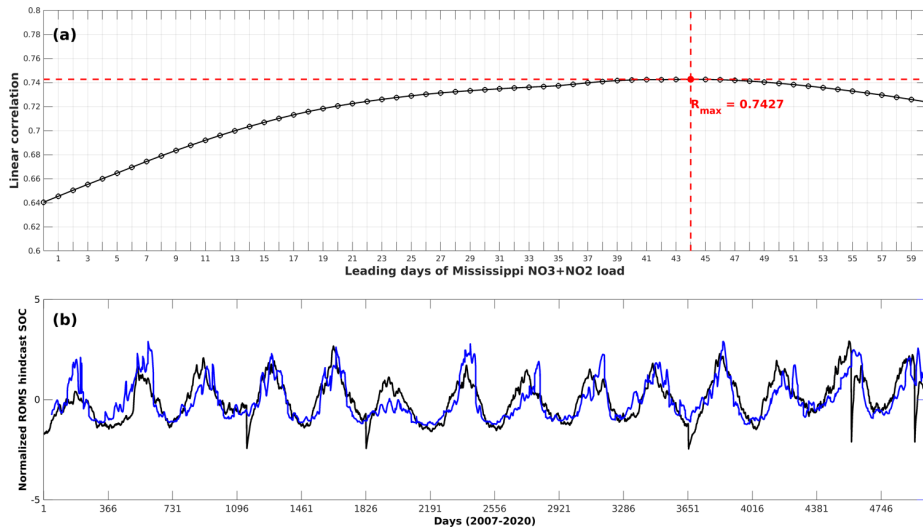
1946

1947 **Figure A2.** A scatter plot of $\rho_a W^3$ against W^3 and their linear correlation.

1948 **Table A1** A correlation matrix of monthly mean inorganic nutrient loads by the Mississippi River and the Atchafalaya River from
1949 **2007 to 2020. Correlation coefficients shown are all significant ($p < 0.001$).**

	Mississippi nitrate+nitrite	Atchafalaya nitrate+nitrite	Mississippi phosphate	Atchafalaya phosphate	Mississippi silicate	Atchafalaya silicate
Mississippi nitrate+nitrite	1					
Atchafalaya nitrate+nitrite	0.9207	1				
Mississippi phosphate	0.8258	0.7551	1			
Atchafalaya phosphate	0.7576	0.7764	0.9308	1		
Mississippi silicate	0.8511	0.7770	0.8664	0.7972	1	
Atchafalaya silicate	0.7989	0.7781	0.8147	0.7942	0.9673	1

1950



Deleted:

Deleted: A2

Deleted: led

Deleted: led

Deleted: 19

Deleted: Time

Deleted: of compared is averaged

Deleted: is

1954

1955

1956

1957

1958

1959 Reference

1960 Battaglin, W. A., Aulenbach, B. T., Vecchia, A., and Buxton, H. T.: Changes in streamflow and the flux of nutrients in the
 1961 Mississippi-Atchafalaya River Basin, USA, 1980-2007, Scientific Investigations Report, Reston, VA,
 1962 <https://doi.org/10.3133/sir20095164>, 2010.

1963 Bianchi, T. S., DiMarco, S. F., Cowan, J. H., Hetland, R. D., Chapman, P., Day, J. W., and Allison, M. A.: The science of
 1964 hypoxia in the northern Gulf of Mexico: A review, *Sci. Total Environ.*, 408, 1471–1484,
 1965 <https://doi.org/10.1016/j.scitotenv.2009.11.047>, 2010.

1966 Bleck, R.: An oceanic general circulation model framed in hybrid isopycnic-Cartesian coordinates, *Ocean Model.*, 4, 55–88,
 1967 [https://doi.org/10.1016/S1463-5003\(01\)00012-9](https://doi.org/10.1016/S1463-5003(01)00012-9), 2002.

1968 Bleck, R. and Boudra, D. B.: Initial testing of a numerical ocean circulation model using a hybrid (quasi-isopycnic) vertical
 1969 coordinate, *J. Phys. Oceanogr.*, 11, 755–770, [https://doi.org/https://doi.org/10.1175/1520-0485\(1981\)011<0755:ITOANO>2.0.CO;2](https://doi.org/https://doi.org/10.1175/1520-0485(1981)011<0755:ITOANO>2.0.CO;2), 1981.

1971 Chesney, E. J. and Baltz, D. M.: The effects of hypoxia on the northern Gulf of Mexico Coastal Ecosystem: A fisheries
 1972 perspective, in: *Coastal Hypoxia: Consequences for Living Resources and Ecosystems*, American Geophysical Union, 321–
 1973 354, <https://doi.org/10.1029/CE058p0321>, 2001.

- 1982 Conley, D. J., Paerl, H. W., Howarth, R. W., Boesch, D. F., Seitzinger, S. P., Havens, K. E., Lancelot, C., and Likens, G. E.:
 1983 Controlling Eutrophication: Nitrogen and Phosphorus, *Science* (80-.), 323, 1014–1015,
 1984 <https://doi.org/10.1126/science.1167755>, 2009.
- 1985 Craig, J. K.: Aggregation on the edge: Effects of hypoxia avoidance on the spatial distribution of brown shrimp and demersal
 1986 fishes in the Northern Gulf of Mexico, *Mar. Ecol. Prog. Ser.*, 445, 75–95, <https://doi.org/10.3354/meps09437>, 2012.
- 1987 Craig, J. K. and Bosman, S. H.: Small Spatial Scale Variation in Fish Assemblage Structure in the Vicinity of the Northwestern
 1988 Gulf of Mexico Hypoxic Zone, 36, 268–285, <https://doi.org/10.1007/s12237-012-9577-9>, 2013.
- 1989 Craig, J. K. and Crowder, L. B.: Hypoxia-induced habitat shifts and energetic consequences in Atlantic croaker and brown
 1990 shrimp on the Gulf of Mexico shelf, *Mar. Ecol. Prog. Ser.*, 294, 79–94, <https://doi.org/10.3354/meps294079>, 2005.
- 1991 Cummings, J. A.: Operational multivariate ocean data assimilation, *Q. J. R. Meteorol. Soc.*, 131, 3583–3604,
 1992 <https://doi.org/10.1256/qj.05.105>, 2005.
- 1993 Cummings, J. A. and Smedstad, O. M.: Variational Data Assimilation for the Global Ocean, in: *Data Assimilation for*
 1994 *Atmospheric, Oceanic and Hydrologic Applications*, vol. II, edited by: Park, S. K. and Xu, L., Springer Berlin Heidelberg,
 1995 303–343, https://doi.org/10.1007/978-3-642-35088-7_13, 2013.
- 1996 Feng, Y., Fennel, K., Jackson, G. A., DiMarco, S. F., and Hetland, R. D.: A model study of the response of hypoxia to
 1997 upwelling-favorable wind on the northern Gulf of Mexico shelf, *J. Mar. Syst.*, 131, 63–73,
 1998 <https://doi.org/10.1016/j.jmarsys.2013.11.009>, 2014.
- 1999 Fennel, K., Hetland, R., Feng, Y., and Dimarco, S.: A coupled physical-biological model of the Northern Gulf of Mexico shelf:
 2000 Model description, validation and analysis of phytoplankton variability, 8, 1881–1899, [https://doi.org/10.5194/bg-8-1881-](https://doi.org/10.5194/bg-8-1881-2011)
 2001 2011, 2011.
- 2002 Fennel, K., Hu, J., Laurent, A., Marta-Almeida, M., and Hetland, R.: Sensitivity of hypoxia predictions for the northern Gulf
 2003 of Mexico to sediment oxygen consumption and model nesting, *J. Geophys. Res. Ocean.*, 118, 990–1002,
 2004 <https://doi.org/10.1002/jgrc.20077>, 2013.
- 2005 Fennel, K., Laurent, A., Hetland, R., Justic, D., Ko, D. S., Lehrter, J., Murrell, M., Wang, L., Yu, L., and Zhang, W.: Effects
 2006 of model physics on hypoxia simulations for the northern Gulf of Mexico: A model intercomparison, *J. Geophys. Res. Ocean.*,
 2007 121, 5731–5750, <https://doi.org/10.1002/2015JC011516>, 2016.
- 2008 Forrest, D. R., Hetland, R. D., and DiMarco, S. F.: Multivariable statistical regression models of the areal extent of hypoxia
 2009 over the Texas-Louisiana continental shelf, *Environ. Res. Lett.*, 6, 045002, <https://doi.org/10.1088/1748-9326/6/4/045002>,
 2010 2011.
- 2011 Del Giudice, D., Matli, V. R. R., and Obenour, D. R.: Bayesian mechanistic modeling characterizes Gulf of Mexico hypoxia:
 2012 1968–2016 and future scenarios, *Ecol. Appl.*, 30, 1–14, <https://doi.org/10.1002/eap.2032>, 2020.
- 2013 Hazen, E. L., Craig, J. K., Good, C. P., and Crowder, L. B.: Vertical distribution of fish biomass in hypoxic waters on the gulf
 2014 of Mexico shelf, *Mar. Ecol. Prog. Ser.*, 375, 195–207, <https://doi.org/10.3354/meps07791>, 2009.
- 2015 Hetland, R. D. and DiMarco, S. F.: How does the character of oxygen demand control the structure of hypoxia on the Texas-
 2016 Louisiana continental shelf?, *J. Mar. Syst.*, 70, 49–62, <https://doi.org/10.1016/j.jmarsys.2007.03.002>, 2008.
- 2017 Jackman, S.: *pscl: Classes and Methods for R Developed in the Political Science Computational Laboratory*,
 2018 <https://github.com/atahk/pscl/>, 2020.

2019 Justić, D. and Wang, L.: Assessing temporal and spatial variability of hypoxia over the inner Louisiana-upper Texas shelf:
2020 Application of an unstructured-grid three-dimensional coupled hydrodynamic-water quality model, *Cont. Shelf Res.*, 72, 163–
2021 179, <https://doi.org/10.1016/j.csr.2013.08.006>, 2014.

2022 Katin, A., Del Giudice, D., and Obenour, D. R.: Temporally resolved coastal hypoxia forecasting and uncertainty assessment
2023 via Bayesian mechanistic modeling, *Hydrol. Earth Syst. Sci.*, 26, 1131–1143, <https://doi.org/10.5194/hess-26-1131-2022>,
2024 2022.

2025 LaBone, E., Rose, K., Justic, D., Huang, H., and Wang, L.: Effects of spatial variability on the exposure of fish to hypoxia: a
2026 modeling analysis for the Gulf of Mexico, *Biogeosciences Discuss.*, 1–35, <https://doi.org/10.5194/bg-2020-51>, 2020.

2027 Lambert, D.: Zero-inflated poisson regression, with an application to defects in manufacturing, 34, 1–14,
2028 <https://doi.org/10.1080/00401706.1992.10485228>, 1992.

2029 Laurent, A. and Fennel, K.: Time-Evolving, Spatially Explicit Forecasts of the Northern Gulf of Mexico Hypoxic Zone,
2030 *Environ. Sci. Technol.*, 53, 14449–14458, <https://doi.org/10.1021/acs.est.9b05790>, 2019.

2031 Laurent, A., Fennel, K., Ko, D. S., and Lehrter, J.: Climate change projected to exacerbate impacts of coastal Eutrophication
2032 in the Northern Gulf of Mexico, *J. Geophys. Res. Ocean.*, 123, 3408–3426, <https://doi.org/10.1002/2017JC013583>, 2018.

2033 Matli, V. R. R., Fang, S., Guinness, J., Rabalais, N. N., Craig, J. K., and Obenour, D. R.: Space-Time Geostatistical Assessment
2034 of Hypoxia in the Northern Gulf of Mexico, *Environ. Sci. Technol.*, 52, 12484–12493, <https://doi.org/10.1021/acs.est.8b03474>,
2035 2018.

2036 Mattern, J. P., Fennel, K., and Dowd, M.: Sensitivity and uncertainty analysis of model hypoxia estimates for the Texas-
2037 Louisiana shelf, *J. Geophys. Res. Ocean.*, 118, 1316–1332, <https://doi.org/10.1002/jgrc.20130>, 2013.

2038 McCarthy, M. J., Carini, S. A., Liu, Z., Ostrom, N. E., and Gardner, W. S.: Oxygen consumption in the water column and
2039 sediments of the northern Gulf of Mexico hypoxic zone, *Estuar. Coast. Shelf Sci.*, 123, 46–53,
2040 <https://doi.org/10.1016/j.ecss.2013.02.019>, 2013.

2041 Mississippi River/Gulf of Mexico Watershed Nutrient Task Force: Action Plan for Reducing, Mitigating, and Controlling
2042 Hypoxia in the Northern Gulf of Mexico, Washington,DC., 2001.

2043 Mississippi River/Gulf of Mexico Watershed Nutrient Task Force: Gulf Hypoxia Action Plan 2008 for Reducing, Mitigating,
2044 and Controlling Hypoxia in the Northern Gulf of Mexico and Improving Water Quality in the Mississippi River Basin,
2045 Washington,DC., 2008.

2046 Monteith, J. and Unsworth, M.: Principles of environmental physics: plants, animals, and the atmosphere, 4th ed., Academic
2047 Press, <https://doi.org/https://doi.org/10.1016/C2010-0-66393-0>, 2014.

2048 Murray, F. W.: On the Computation of Saturation Vapor Pressure, *J. Appl. Meteorol. Climatol.*, 6, 203–204,
2049 [https://doi.org/https://doi.org/10.1175/1520-0450\(1967\)006<0203:OTCOSV>2.0.CO;2](https://doi.org/https://doi.org/10.1175/1520-0450(1967)006<0203:OTCOSV>2.0.CO;2), 1967.

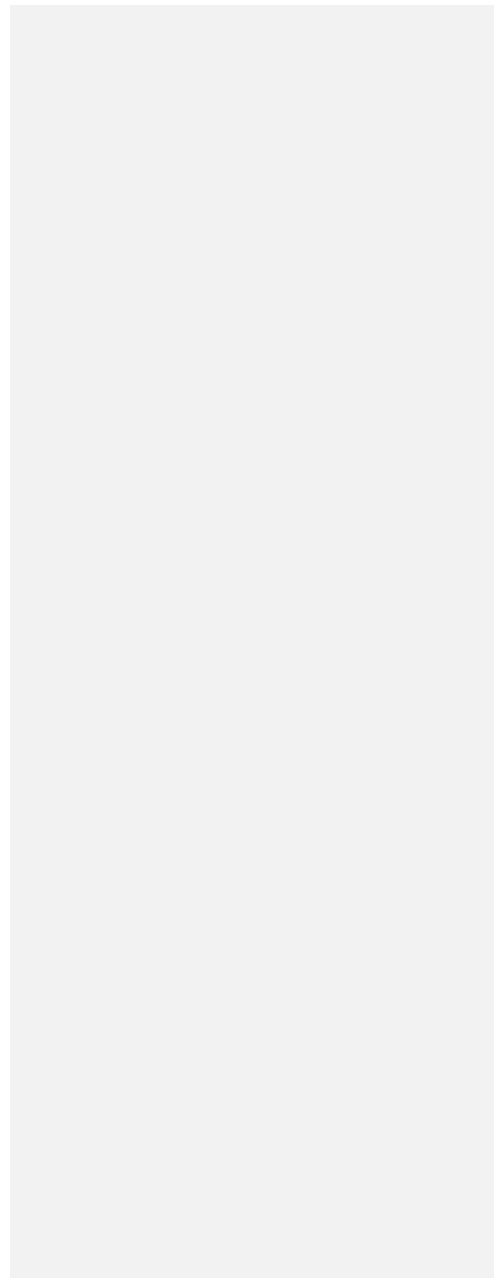
2050 Murrell, M. C. and Lehrter, J. C.: Sediment and Lower Water Column Oxygen Consumption in the Seasonally Hypoxic Region
2051 of the Louisiana Continental Shelf, 34, 912–924, <https://doi.org/10.1007/s12237-010-9351-9>, 2011.

2052 de Mutsert, K., Steenbeek, J., Lewis, K., Buszowski, J., Cowan, J. H., and Christensen, V.: Exploring effects of hypoxia on
2053 fish and fisheries in the northern Gulf of Mexico using a dynamic spatially explicit ecosystem model, *Ecol. Modell.*, 331, 142–
2054 150, <https://doi.org/10.1016/j.ecolmodel.2015.10.013>, 2016.

2055 Obenour, D. R., Michalak, A. M., and Scavia, D.: Assessing biophysical controls on Gulf of Mexico hypoxia through

- 2056 probabilistic modeling, *Ecol. Appl.*, 25, 492–505, <https://doi.org/10.1890/13-2257.1>, 2015.
- 2057 Picard, A., Davis, R. S., Gläser, M., and Fujii, K.: Revised formula for the density of moist air (CIPM-2007), 45, 149–155,
2058 <https://doi.org/10.1088/0026-1394/45/2/004>, 2008.
- 2059 Purcell, K. M., Craig, J. K., Nance, J. M., Smith, M. D., and Benneer, L. S.: Fleet behavior is responsive to a large-scale
2060 environmental disturbance: Hypoxia effects on the spatial dynamics of the northern Gulf of Mexico shrimp fishery,
2061 <https://doi.org/10.1371/journal.pone.0183032>, 2017.
- 2062 Rabalais, N. N. and Baustian, M. M.: Historical Shifts in Benthic Infaunal Diversity in the Northern Gulf of Mexico since the
2063 Appearance of Seasonally Severe Hypoxia, 12, <https://doi.org/10.3390/d12020049>, 2020.
- 2064 Rabalais, N. N. and Turner, R. E.: Gulf of Mexico Hypoxia: Past, Present, and Future, *Limnol. Oceanogr. Bull.*, 28, 117–124,
2065 <https://doi.org/10.1002/lob.10351>, 2019.
- 2066 Rabalais, N. N., Turner, R. E., and Wiseman, W. J.: Gulf of Mexico hypoxia, a.k.a. “The dead zone,” *Annu. Rev. Ecol. Syst.*,
2067 33, 235–263, <https://doi.org/10.1146/annurev.ecolsys.33.010802.150513>, 2002.
- 2068 Rabalais, N. N., Turner, R. E., Sen Gupta, B. K., Boesch, D. F., Chapman, P., and Murrell, M. C.: Hypoxia in the northern
2069 Gulf of Mexico: Does the science support the plan to reduce, mitigate, and control hypoxia?, 30, 753–772,
2070 <https://doi.org/10.1007/BF02841332>, 2007a.
- 2071 Rabalais, N. N., Turner, R. E., Gupta, B. K. S., Platon, E., and Parsons, M. L.: Sediments tell the history of eutrophication and
2072 hypoxia in the northern Gulf of Mexico, *Ecol. Appl.*, 17, 129–143, <https://doi.org/10.1890/06-0644.1>, 2007b.
- 2073 Rabotyagov, S. S., Kling, C. L., Gassman, P. W., Rabalais, N. N., and Turner, R. E.: The economics of dead zones: Causes,
2074 impacts, policy challenges, and a model of the gulf of Mexico Hypoxic Zone, *Rev. Environ. Econ. Policy*, 8, 58–79,
2075 <https://doi.org/10.1093/reep/ret024>, 2014.
- 2076 Reyes, B. A., Pendergast, J. S., and Yamazaki, S.: Mammalian peripheral circadian oscillators are temperature compensated,
2077 *J. Biol. Rhythms*, 23, 95–98, <https://doi.org/10.1177/0748730407311855>, 2008.
- 2078 Saha, S., Moorthi, S., Pan, H.-L., Wu, X., Wang, J., Nadiga, S., Tripp, P., Kistler, R., Woollen, J., Behringer, D., Liu, H.,
2079 Stokes, D., Grumbine, R., Gayno, G., Wang, J., Hou, Y.-T., Chuang, H.-Y., Juang, H.-M. H., Sela, J., Iredell, M., Treadon, R.,
2080 Kleist, D., Van Delst, P., Keyser, D., Derber, J., Ek, M., Meng, J., Wei, H., Yang, R., Lord, S., van den Dool, H., Kumar, A.,
2081 Wang, W., Long, C., Chelliah, M., Xue, Y., Huang, B., Schemm, J.-K., Ebisuzaki, W., Lin, R., Xie, P., Chen, M., Zhou, S.,
2082 Higgins, W., Zou, C.-Z., Liu, Q., Chen, Y., Han, Y., Cucurull, L., Reynolds, R. W., Rutledge, G., and Goldberg, M.: NCEP
2083 Climate Forecast System Reanalysis (CFSR) 6-hourly Products, January 1979 to December 2010,
2084 <https://doi.org/10.5065/D69K487J>, 2010.
- 2085 Saha, S., Moorthi, S., Wu, X., Wang, J., Nadiga, S., Tripp, P., Behringer, D., Hou, Y.-T., Chuang, H., Iredell, M., Ek, M.,
2086 Meng, J., Yang, R., Mendez, M. P., van den Dool, H., Zhang, Q., Wang, W., Chen, M., and Becker, E.: NCEP Climate Forecast
2087 System Version 2 (CFSv2) 6-hourly Products, <https://doi.org/10.5065/D61C1TXF>, 2011.
- 2088 Scavia, D., Evans, M. A., and Obenour, D. R.: A scenario and forecast model for gulf of mexico hypoxic area and volume,
2089 *Environ. Sci. Technol.*, 47, 10423–10428, <https://doi.org/10.1021/es4025035>, 2013.
- 2090 Scavia, D., Bertani, I., Obenour, D. R., Turner, R. E., Forrest, D. R., and Katin, A.: Ensemble modeling informs hypoxia
2091 management in the northern Gulf of Mexico, *Proc. Natl. Acad. Sci. U. S. A.*, 114, 8823–8828,
2092 <https://doi.org/10.1073/pnas.1705293114>, 2017.
- 2093 Siegel, A. F. and Wagner, M. R.: Chapter 12 - Multiple Regression: Predicting One Variable From Several Others, in: *Practical*

- 2094 Business Statistics, edited by: Siegel, A. F. and Wagner, M. R., 371–431, <https://doi.org/https://doi.org/10.1016/B978-0-12-820025-4.00012-9>, 2022.
- 2096 Simpson, J. H.: The shelf-sea fronts: implications of their existence and behaviour, *Philos. Trans. R. Soc. London. Ser. A, Math. Phys. Sci.*, 302, 531–546, <https://doi.org/10.1098/rsta.1981.0181>, 1981.
- 2098 Simpson, J. H. and Bowers, D.: Models of stratification and frontal movement in shelf seas, *Deep Sea Res. Part A, Oceanogr. Res. Pap.*, 28, 727–738, [https://doi.org/10.1016/0198-0149\(81\)90132-1](https://doi.org/10.1016/0198-0149(81)90132-1), 1981.
- 2100 Simpson, J. H. and Hunter, J. R.: Fronts in the Irish Sea, *Nature*, 250, 404–406, <https://doi.org/10.1038/250404a0>, 1974.
- 2101 Simpson, J. H., Allen, C. M., and Morris, N. C. G.: Fronts on the Continental Shelf, *J. Geophys. Res.*, 83, 4607–4614, <https://doi.org/10.1029/JC083iC09p04607>, 1978.
- 2103 Smith, M. D., Asche, F., Benneer, L. S., and Oglend, A.: Spatial-dynamics of hypoxia and fisheries: The case of Gulf of Mexico brown shrimp, *Mar. Resour. Econ.*, 29, 111–131, <https://doi.org/10.1086/676826>, 2014.
- 2105 Turner, R. E., Rabalais, N. N., and Justic, D.: Predicting summer hypoxia in the northern Gulf of Mexico: Riverine N, P, and Si loading, *Mar. Pollut. Bull.*, 52, 139–148, <https://doi.org/10.1016/j.marpolbul.2005.08.012>, 2006.
- 2107 Turner, R. E., Rabalais, N. N., and Justic, D.: Gulf of Mexico hypoxia: Alternate states and a legacy, *Environ. Sci. Technol.*, 42, 2323–2327, <https://doi.org/10.1021/es071617k>, 2008.
- 2109 Turner, R. E., Rabalais, N. N., and Justić, D.: Predicting summer hypoxia in the northern Gulf of Mexico: Redux, *Mar. Pollut. Bull.*, 64, 319–324, <https://doi.org/10.1016/j.marpolbul.2011.11.008>, 2012.
- 2111 van't Hoff, J. H. and Leffeldt, R. A.: Lectures in theoretical and physical chemistry: Part I: Chemical dynamics, London: Edward Arnold, London, 1899.
- 2113 Venables, W. N. and Ripley, B. D.: *Modern Applied Statistics with S*, Fourth., Springer, New York, <https://doi.org/10.1007/978-0-387-21706-2>, 2002.
- 2115 Wang, L. and Justić, D.: A modeling study of the physical processes affecting the development of seasonal hypoxia over the inner Louisiana-Texas shelf: Circulation and stratification, *Cont. Shelf Res.*, 29, 1464–1476, <https://doi.org/10.1016/j.csr.2009.03.014>, 2009.
- 2118 Warner, J. C., Armstrong, B., He, R., and Zambon, J. B.: Development of a Coupled Ocean-Atmosphere-Wave-Sediment Transport (COAWST) Modeling System, *Ocean Model.*, 35, 230–244, <https://doi.org/10.1016/j.ocemod.2010.07.010>, 2010.
- 2120 Wood, S. N.: Thin plate regression splines, *J. R. Stat. Soc. Ser. B Stat. Methodol.*, 65, 95–114, <https://doi.org/10.1111/1467-9868.00374>, 2003.
- 2122 Wood, S. N.: Fast stable restricted maximum likelihood and marginal likelihood estimation of semiparametric generalized linear models, *J. R. Stat. Soc. Ser. B Stat. Methodol.*, 73, 3–36, <https://doi.org/10.1111/j.1467-9868.2010.00749.x>, 2011.
- 2124 Yu, L., Fennel, K., and Laurent, A.: A modeling study of physical controls on hypoxia generation in the northern Gulf of Mexico, *J. Geophys. Res. Ocean.*, 120, 5019–5039, <https://doi.org/10.1002/2014JC010634>, 2015.
- 2126 Zambresky, L.: A verification study of the global WAM model, December 1987 – November 1988, 1989.
- 2127 Zeileis, A., Kleiber, C., and Jackman, S.: Regression Models for Count Data in R, *J. Stat. Softw.*, 27, <https://doi.org/10.18637/jss.v027.i08>, 2008.



Page 3: [1] Deleted Yanda Ou 6/6/22 11:53:00 AM

Page 3: [1] Deleted Yanda Ou 6/6/22 11:53:00 AM

Page 3: [1] Deleted Yanda Ou 6/6/22 11:53:00 AM

Page 3: [2] Deleted Z. George Xue 6/6/22 11:53:00 AM

Page 3: [2] Deleted Z. George Xue 6/6/22 11:53:00 AM

Page 3: [3] Deleted Yanda Ou 6/6/22 11:53:00 AM

Page 3: [3] Deleted Yanda Ou 6/6/22 11:53:00 AM

Page 3: [4] Deleted Z. George Xue 6/13/22 10:52:00 AM

Page 3: [4] Deleted Z. George Xue 6/13/22 10:52:00 AM

Page 3: [5] Deleted Yanda Ou 6/6/22 11:53:00 AM

Page 3: [5] Deleted Yanda Ou 6/6/22 11:53:00 AM

Page 3: [6] Deleted Z. George Xue 6/13/22 11:01:00 AM

Page 3: [6] Deleted Z. George Xue 6/13/22 11:01:00 AM

Page 3: [6] Deleted Z. George Xue 6/13/22 11:01:00 AM

Page 3: [7] Deleted Z. George Xue 6/13/22 10:52:00 AM

Page 3: [7] Deleted Z. George Xue 6/13/22 10:52:00 AM

Page 3: [8] Deleted Yanda Ou 6/6/22 11:53:00 AM

Page 3: [8] Deleted Yanda Ou 6/6/22 11:53:00 AM

Page 3: [8] Deleted Yanda Ou 6/6/22 11:53:00 AM

Page 3: [9] Deleted Z. George Xue 6/13/22 11:02:00 AM

Page 3: [10] Deleted Yanda Ou 6/6/22 11:53:00 AM

Page 3: [10] Deleted Yanda Ou 6/6/22 11:53:00 AM

Page 3: [10] Deleted Yanda Ou 6/6/22 11:53:00 AM

Page 3: [10] Deleted Yanda Ou 6/6/22 11:53:00 AM

Page 3: [11] Deleted Z. George Xue 6/13/22 10:57:00 AM

Page 3: [11] Deleted Z. George Xue 6/13/22 10:57:00 AM

Page 3: [12] Deleted Yanda Ou 6/14/22 10:51:00 AM

Page 3: [12] Deleted Yanda Ou 6/14/22 10:51:00 AM

Page 3: [12] Deleted Yanda Ou 6/14/22 10:51:00 AM

Page 3: [12] Deleted Yanda Ou 6/14/22 10:51:00 AM

Page 3: [12] Deleted Yanda Ou 6/14/22 10:51:00 AM

Page 3: [13] Deleted Yanda Ou 6/9/22 10:23:00 AM

▼
Page 6: [15] Deleted Z. George Xue 6/13/22 1:15:00 PM

▼
Page 6: [15] Deleted Z. George Xue 6/13/22 1:15:00 PM

▼
Page 6: [15] Deleted Z. George Xue 6/13/22 1:15:00 PM

▼
Page 6: [16] Deleted Yanda Ou 6/14/22 10:57:00 AM

▼
Page 6: [16] Deleted Yanda Ou 6/14/22 10:57:00 AM

▼
Page 6: [17] Deleted Z. George Xue 6/13/22 1:16:00 PM

▼
Page 6: [17] Deleted Z. George Xue 6/13/22 1:16:00 PM

▼
Page 6: [17] Deleted Z. George Xue 6/13/22 1:16:00 PM

▼
Page 6: [17] Deleted Z. George Xue 6/13/22 1:16:00 PM

▼
Page 6: [18] Deleted Yanda Ou 6/9/22 10:50:00 AM

▼
Page 6: [18] Deleted Yanda Ou 6/9/22 10:50:00 AM

▼
Page 6: [18] Deleted Yanda Ou 6/9/22 10:50:00 AM

▼
Page 6: [18] Deleted Yanda Ou 6/9/22 10:50:00 AM

▼
Page 6: [18] Deleted Yanda Ou 6/9/22 10:50:00 AM

▼
Page 6: [18] Deleted Yanda Ou 6/9/22 10:50:00 AM

▼
Page 6: [18] Deleted Yanda Ou 6/9/22 10:50:00 AM

Page 6: [18] Deleted Yanda Ou 6/9/22 10:50:00 AM

Page 6: [19] Deleted Yanda Ou 6/6/22 11:53:00 AM

Page 6: [19] Deleted Yanda Ou 6/6/22 11:53:00 AM

Page 6: [20] Deleted Yanda Ou 6/6/22 11:53:00 AM

Page 6: [20] Deleted Yanda Ou 6/6/22 11:53:00 AM

Page 6: [20] Deleted Yanda Ou 6/6/22 11:53:00 AM

Page 6: [21] Deleted Yanda Ou 6/6/22 11:53:00 AM

Page 6: [21] Deleted Yanda Ou 6/6/22 11:53:00 AM

Page 6: [21] Deleted Yanda Ou 6/6/22 11:53:00 AM

Page 6: [21] Deleted Yanda Ou 6/6/22 11:53:00 AM

Page 6: [21] Deleted Yanda Ou 6/6/22 11:53:00 AM

Page 6: [21] Deleted Yanda Ou 6/6/22 11:53:00 AM

Page 6: [21] Deleted Yanda Ou 6/6/22 11:53:00 AM

Page 6: [22] Deleted Yanda Ou 6/6/22 11:53:00 AM

Page 6: [22] Deleted Yanda Ou 6/6/22 11:53:00 AM

Page 6: [23] Deleted Yanda Ou 6/15/22 10:29:00 AM

Page 6: [23] Deleted Yanda Ou 6/15/22 10:29:00 AM

Page 19: [24] Deleted Z. George Xue 6/13/22 1:49:00 PM

Page 19: [24] Deleted Z. George Xue 6/13/22 1:49:00 PM

Page 19: [24] Deleted Z. George Xue 6/13/22 1:49:00 PM

Page 19: [24] Deleted Z. George Xue 6/13/22 1:49:00 PM

Page 19: [24] Deleted Z. George Xue 6/13/22 1:49:00 PM

Page 19: [24] Deleted Z. George Xue 6/13/22 1:49:00 PM

Page 19: [24] Deleted Z. George Xue 6/13/22 1:49:00 PM

Page 19: [24] Deleted Z. George Xue 6/13/22 1:49:00 PM

Page 19: [24] Deleted Z. George Xue 6/13/22 1:49:00 PM

Page 19: [24] Deleted Z. George Xue 6/13/22 1:49:00 PM

Page 19: [24] Deleted Z. George Xue 6/13/22 1:49:00 PM

Page 19: [24] Deleted Z. George Xue 6/13/22 1:49:00 PM

Page 19: [24] Deleted Z. George Xue 6/13/22 1:49:00 PM

Page 19: [24] Deleted Z. George Xue 6/13/22 1:49:00 PM

Page 19: [24] Deleted Z. George Xue 6/13/22 1:49:00 PM

▼
Page 19: [24] Deleted Z. George Xue 6/13/22 1:49:00 PM

▼
Page 23: [25] Deleted Z. George Xue 6/14/22 9:13:00 AM

▼
Page 23: [26] Deleted Z. George Xue 6/14/22 9:14:00 AM

▼
Page 24: [27] Deleted Z. George Xue 6/14/22 9:15:00 AM

▼
Page 24: [27] Deleted Z. George Xue 6/14/22 9:15:00 AM

▼
Page 24: [28] Deleted Z. George Xue 6/14/22 9:15:00 AM

▼
Page 24: [28] Deleted Z. George Xue 6/14/22 9:15:00 AM

▼
Page 24: [28] Deleted Z. George Xue 6/14/22 9:15:00 AM

▼
Page 24: [29] Deleted Z. George Xue 6/14/22 9:18:00 AM

▼
Page 24: [29] Deleted Z. George Xue 6/14/22 9:18:00 AM

▼
Page 24: [29] Deleted Z. George Xue 6/14/22 9:18:00 AM

▼
Page 24: [29] Deleted Z. George Xue 6/14/22 9:18:00 AM

▼
Page 24: [29] Deleted Z. George Xue 6/14/22 9:18:00 AM

▼
Page 24: [29] Deleted Z. George Xue 6/14/22 9:18:00 AM

▼
Page 24: [29] Deleted Z. George Xue 6/14/22 9:18:00 AM

▼
Page 24: [29] Deleted Z. George Xue 6/14/22 9:18:00 AM

Page 24: [29] Deleted Z. George Xue 6/14/22 9:18:00 AM

Page 24: [29] Deleted Z. George Xue 6/14/22 9:18:00 AM

Page 24: [29] Deleted Z. George Xue 6/14/22 9:18:00 AM

Page 24: [29] Deleted Z. George Xue 6/14/22 9:18:00 AM

Page 24: [29] Deleted Z. George Xue 6/14/22 9:18:00 AM

Page 24: [29] Deleted Z. George Xue 6/14/22 9:18:00 AM

Page 24: [30] Deleted Yanda Ou 6/15/22 4:02:00 PM

Page 24: [30] Deleted Yanda Ou 6/15/22 4:02:00 PM

Page 24: [31] Deleted Z. George Xue 6/14/22 9:21:00 AM

Page 24: [31] Deleted Z. George Xue 6/14/22 9:21:00 AM

Page 24: [31] Deleted Z. George Xue 6/14/22 9:21:00 AM

Page 24: [32] Deleted Z. George Xue 6/14/22 9:22:00 AM

Page 24: [32] Deleted Z. George Xue 6/14/22 9:22:00 AM

Page 24: [33] Deleted Z. George Xue 6/14/22 9:25:00 AM

Page 24: [33] Deleted Z. George Xue 6/14/22 9:25:00 AM

Page 24: [33] Deleted Z. George Xue 6/14/22 9:25:00 AM

Page 24: [33] Deleted Z. George Xue 6/14/22 9:25:00 AM

Page 24: [33] Deleted Z. George Xue 6/14/22 9:25:00 AM

Page 24: [33] Deleted Z. George Xue 6/14/22 9:25:00 AM

Page 24: [33] Deleted Z. George Xue 6/14/22 9:25:00 AM

Page 24: [33] Deleted Z. George Xue 6/14/22 9:25:00 AM

Page 24: [33] Deleted Z. George Xue 6/14/22 9:25:00 AM

Page 24: [33] Deleted Z. George Xue 6/14/22 9:25:00 AM

Page 24: [33] Deleted Z. George Xue 6/14/22 9:25:00 AM

Page 24: [33] Deleted Z. George Xue 6/14/22 9:25:00 AM

Page 25: [34] Deleted Z. George Xue 6/14/22 9:36:00 AM

Page 25: [35] Deleted Z. George Xue 6/14/22 9:37:00 AM

Page 25: [35] Deleted Z. George Xue 6/14/22 9:37:00 AM

Page 25: [35] Deleted Z. George Xue 6/14/22 9:37:00 AM

Page 25: [36] Deleted Z. George Xue 6/14/22 9:39:00 AM

Page 25: [36] Deleted Z. George Xue 6/14/22 9:39:00 AM

Page 25: [37] Deleted Z. George Xue 6/14/22 9:40:00 AM

Page 25: [37] Deleted Z. George Xue 6/14/22 9:40:00 AM

Page 25: [37] Deleted Z. George Xue 6/14/22 9:40:00 AM

Page 25: [38] Deleted Yanda Ou 6/14/22 12:17:00 PM

Page 25: [38] Deleted Yanda Ou 6/14/22 12:17:00 PM

Page 25: [39] Deleted Z. George Xue 6/14/22 9:46:00 AM

Page 25: [39] Deleted Z. George Xue 6/14/22 9:46:00 AM

Page 25: [39] Deleted Z. George Xue 6/14/22 9:46:00 AM

Page 25: [39] Deleted Z. George Xue 6/14/22 9:46:00 AM

Page 25: [40] Deleted Yanda Ou 6/6/22 11:53:00 AM

Page 25: [40] Deleted Yanda Ou 6/6/22 11:53:00 AM

Page 25: [40] Deleted Yanda Ou 6/6/22 11:53:00 AM

Page 25: [40] Deleted Yanda Ou 6/6/22 11:53:00 AM

Page 25: [40] Deleted Yanda Ou 6/6/22 11:53:00 AM

Page 25: [40] Deleted Yanda Ou 6/6/22 11:53:00 AM

Page 25: [40] Deleted Yanda Ou 6/6/22 11:53:00 AM

Page 25: [40] Deleted Yanda Ou 6/6/22 11:53:00 AM

Page 25: [40] Deleted Yanda Ou 6/6/22 11:53:00 AM

Page 25: [41] Deleted Z. George Xue 6/14/22 9:48:00 AM

Page 25: [41] Deleted Z. George Xue 6/14/22 9:48:00 AM

Page 25: [41] Deleted Z. George Xue 6/14/22 9:48:00 AM

Page 25: [41] Deleted Z. George Xue 6/14/22 9:48:00 AM

Page 25: [42] Deleted Z. George Xue 6/14/22 9:49:00 AM

Page 25: [42] Deleted Z. George Xue 6/14/22 9:49:00 AM

Page 25: [42] Deleted Z. George Xue 6/14/22 9:49:00 AM

Page 25: [42] Deleted Z. George Xue 6/14/22 9:49:00 AM

Page 25: [42] Deleted Z. George Xue 6/14/22 9:49:00 AM

Page 25: [42] Deleted Z. George Xue 6/14/22 9:49:00 AM

Page 25: [42] Deleted Z. George Xue 6/14/22 9:49:00 AM

Page 25: [42] Deleted Z. George Xue 6/14/22 9:49:00 AM

Page 25: [42] Deleted Z. George Xue 6/14/22 9:49:00 AM

Page 25: [43] Deleted Yanda Ou 6/14/22 12:18:00 PM

Page 25: [43] Deleted Yanda Ou 6/14/22 12:18:00 PM

Page 25: [43] Deleted Yanda Ou 6/14/22 12:18:00 PM

